Electron-energy-loss spectroscopy of H adsorbed on Rh(100): Interpretation of overtone spectra as two-phonon bound states

Lee J. Richter,* Thomas A. Germer, James P. Sethna, and W. Ho
Laboratory of Atomic and Solid State Physics and Materials Science Center, Cornell University, Ithaca, New York 14853
(Received 9 February 1988)

The vibrational properties of H adsorbed in the fourfold-hollow site on Rh(100) have been studied with high-resolution electron-energy-loss spectroscopy. At saturation coverage (one H per Rh atom), proper selection of the incident-electron energy and collection angle of the scattered electrons allow the detection of the symmetric (perpendicular) and asymmetric (degenerate parallel) fundamental transitions and five overtone transitions. The fundamental transitions exhibit significant frequency shifts as the H coverage is changed, establishing that H-H interactions are important in determining the local curvature of the adsorption potential-energy surface. Spectra of isotopically mixed layers (H and D) establish that significant dynamic coupling exists in both the parallel and perpendicular states at 1.0 monolayer coverage. The phonon bandwidths estimated from the isotope dilution experiments are 12–15 meV. The dynamic coupling is comparable to the local anharmonicity of the vibrational potential, and the overtones correspond to two-phonon bound-state excitations. A one-dimensional model of coupled, anharmonic oscillators is used to guide the interpretation of the overtone spectra. A qualitative interpretation of the spectra requires a proper accounting of the dispersion of both the fundamental and overtone excitations and indicates that the predominantly parallel polarized vibrations are extremely anharmonic, and the predominantly vertical polarized vibrations are only mildly anharmonic. Quantitative determination of the local anharmonicity requires a more detailed description of the H-H coupling than is currently available as the dispersion and anharmonicity are comparable.

I. INTRODUCTION

Vibrational spectroscopy is one of the most important tools available for the study of species adsorbed on surfaces.[1–3] This arises from the wealth of qualitative and quantitative information that can be obtained from vibrational spectra. The number of observed inelastic transitions, coupled with the selection rules relevant to a given spectroscopic technique determine the adsorbate symmetry. When this information is combined with comparisons to model compounds and theoretical calculations, the specific adsorption site often can be established. In addition, a variety of empirical models for vibrational potentials exist which provide qualitative and quantitative insight into the geometry and binding energy of the adsorbate. High-resolution electron-energy-loss spectroscopy (HREELS) has been extraordinarily successful in the characterization of adsorbate vibrational spectra. The advantages of HREELS are its wide spectral range (25–500 meV), high sensitivity, and the richness of the scattering mechanism. By changing the experimental conditions (energy and parallel momentum of the incident electrons, parallel momentum of the detected electrons) inelastic transitions due to excitation of vibrational modes of different polarizations can be observed.[1] Thus HREELS provides information analogous to both infrared absorption and Raman scattering with a single experimental apparatus.

One of the most extensively studied adsorbate systems is hydrogen on the transition metals. The properties of adsorbed H are important to technologies as diverse as heterogeneous catalysis, metallurgy, and energy storage. Chemisorbed H is also of great interest due to its stark simplicity; the low nuclear change, Z, of the species facilitates an understanding of the electronic interaction potential. Recent *ab initio* calculations using linear–augmented-plane-wave (LAPW) and pseudopotential local basis methods have achieved remarkable success in describing the vibrational[4–10] and electronic[11,12] properties of adsorbed H. Unfortunately, the experimental characterization of adsorbed H is difficult since the low Z and light mass result in weak interactions with most surface-sensitive probes. HREELS has provided critical insights into the properties of adsorbed H as it possesses sensitivity sufficient for the study of submonolayer coverages. The relationship between HREELS and the study of H has been symbiotic, as important insights into the physical nature of the inelastic scattering of low-energy electrons have become apparent in the study of chemisorbed H. HREELS studies of the adsorption of H/W(100) (Ref. 13) were the first to demonstrate the importance of impact scattering, establishing the detectability of nondipole-active transitions and the presence of enhancement of the inelastic cross sections at conditions appropriate to the excitation of surface resonances. By carefully optimizing the experimental conditions, not only all of the fundamental losses, but up to three overtone transitions have been observed for H/Ru(001) (Ref. 14) and H/Pd(111) (Ref. 15). This presents the exciting possibility of experimentally determining the "texture" of

the adsorption potential by analyzing the anharmonicity of the vibrational transitions. Improvements in inelastic neutron scattering (INS) have allowed the determination of the anharmonicity of the local H vibrations in metal hydrides,[16,17] significantly advancing the understanding of the H-metal potential. This understanding has recently been highlighted by an accurate first-principles calculation of both the fundamental and overtone transitions for Nb hydride.[18]

We report the first detailed HREELS investigation of the vibrational spectra of H adsorbed on a Rh(100) surface. Unlike previous studies of H/Ni(100), where only one fundamental of H adsorbed in a fourfold hollow was observed,[19] and H/Pd(100), where both fundamentals, but no overtones were observed,[20] we have observed both fundamental transitions and, at high coverage, five overtone transitions. The vibrational loss frequencies change substantially with H coverage. By performing isotope-dilution experiments, it is established that dynamic coupling between the H is a significant source of the coverage dependence of the loss frequencies and that dynamic coupling of H at high coverages is a general feature of H vibrational spectra. Existing models for uncoupled anharmonic oscillators are inadequate for even a qualitative interpretation of the high-coverage spectra as is established by a simple one-dimensional (1D) model of coupled, anharmonic oscillators. Dynamic coupling causes the one-quantum excitations of the anharmonic oscillators to become phonons, extended excitations, with anharmonically shifted frequencies. The anharmonic overtone becomes a unique, two-phonon bound state of the coupled system, with qualitatively different behavior than one- and two-phonon excitations. From the model it is clear that quantitative analysis of the local site anharmonicity cannot be performed without a quantitative model of the oscillator coupling. We are, however, able to draw qualitative conclusions concerning the shape of the vibrational potential well.

The rest of the paper is organized as follows: In Sec. II we outline the experimental procedures used in obtaining the results presented in Sec. III. Section III also presents the assignment of the fundamental transitions. The discussion (Sec. IV) is divided into three parts. In Sec. IV A we discuss the coverage dependence of the fundamental transitions and the evidence for dynamic coupling at high coverages. The model of a 1D chain of linearly coupled, anharmonic oscillators is developed in Sec. IV B. The high-coverage Bloch bound-state ("overtone") transitions are interpreted in Sec. IV C in light of the essential features of the model.

II. EXPERIMENTAL DETAILS

The experiments were performed in a two-tier ultrahigh-vacuum (UHV) chamber providing facilities for ion bombardment, gas dosing, and thermal-desorption spectroscopy (TDS) in the upper level, and HREELS in the lower level.[21] The HREEL spectrometer[22] contains double-pass 127° electrostatic deflectors in both the monochromator and analyzer and has a fixed scattering angle of 120°. Off-specular measurements were performed by rotating the crystal about an axis perpendicular to the scattering plane. The angle ($\Delta\theta$) between the specular direction and the collection axis in the scattering plane is positive towards the surface plane. The reported incident energies (E_i) are computed from the cathode bias voltage corrected for work functions. The small work-function change due to H adsorption (0.2 eV at saturation) was estimated from the shift in the position of extrema in the specular reflectivity associated with the emergence of the first low-energy electron-diffraction (LEED) beam. The work-function change determined in this fashion is consistent with the earlier report of Peebles *et al.*[23] The intensities of the H-derived losses are weak, requiring the resolution of the spectrometer to be degraded to 8–10 meV full width at half maximum (FWHM) in order to obtain adequate statistics. At these resolutions, the specularly scattered ($\Delta\theta=0°$) elastic beam saturated the electron multiplier, except at impact energies associated with deep minima in the reflectivity.

When displaying spectra, both the actual data (points) and cubic-spline-smoothed data (lines) are used (see Fig. 1). The reported loss energies, intensities, and widths were determined by weighted nonlinear least-squares (NLS) fits of region of the EEL spectrum to a sum of up to four Gaussians and a constant, linear, or quadratic background. A modified Marquardt algorithm, incorporating parameter limits,[24] was used for the NLS fits, and the weights were determined by the Poisson statistics of the detected electrons; χ^2 per degree of freedom was typically between 0.9 and 1.1. Except where noted, the uncertainties in reported values are the mean and variance in the mean calculated from data taken at many impact energies and collection angles. A minimum of five, typically 15, spectra at optimal conditions were included in each average.

The Rh crystal, a 1-cm diam, 2-mm-thick disk, was cut and polished to within 0.5° of the (100) orientation and mounted with the scattering plane nominally along the [001] direction. The sample manipulator is of the rotating Dewar style[25] and provides rapid cooling to 85–90 K. Except where noted, all HREEL spectra were recorded at or below 90 K, as were all gas exposures. The Rh(100) crystal has been used in many previous UHV studies; cleaning for a number of years by oxidation-reduction treatments and ion bombardment has depleted all near-surface impurities. The surface was cleaned between spectra by Ne^+ bombardment (500 eV, 1×10^{-5} A) and thermal annealing at 750 K. Cleanliness was established by the reproducibility of known TDS features and HREELS.

The reagents were research-purity H_2 and Ne and commercial purity (99.5%) D_2 from Matheson Gas Products and used as-received. Exposures were performed by backfilling the upper chamber via a variable leak valve and were based on uncorrected ion-gauge readings. Isotopically mixed surfaces were prepared by exposure to the appropriate H_2 and D_2 mixture. The spectrometer was isolated from the upper chamber during exposures to ensure stable surface potentials on the electron optics. H and D coverages were determined by the integrated area under TD spectra. The H_2 dissociative sticking

coefficient is high; an exposure of 2 L (1 L = 1 langmuir or 10^{-6} Torr sec) is sufficient to saturate the surface within experimental accuracy. Kim *et al.*[26] assigned the saturation coverage a value of 1 monolayer (ML) (1 ML $=1.39\times10^{15}$ cm^{-2}), consistent with the high specular reflectivity (indicative of a well-ordered adlayer) observed at saturation by HREELS, the absence of fractional order spots in LEED,[27] and the value of 1.0±0.1 ML determined by elastic recoil scattering for the analogous system of H/Pd(100).[28] The principal component of the background gas was hydrogen. The long data-acquisition times (typically 55 min) required by the weak intensity of the H modes and the high H sticking coefficient resulted in a practical minimum of H coverage of 0.3 ML at 90 K. The maximum D concentration on a surface after a D_2 saturation exposure was ≈85%, the remaining 15% of the (1×1) saturation layer was H.

III. EXPERIMENTAL RESULTS

A. Principal loss features and assignment

Figure 1 displays HREEL spectra of a H-saturated surface taken at $E_i=5.85$ eV as a function of the mean collection angle. Specular collection ($\Delta\theta=0°$) produces spectra characterized by a loss at 82 meV and a weak, broad feature centered at 154 meV. The losses above 230 meV are due to trace amounts (less than 0.02 ML) of adsorbed CO. As the collection angle is moved away from specular, the 82-meV loss rapidly decreases in intensity (note the changes of scale in Fig. 1), as does the center of the 154-meV feature. Spectra taken at $\Delta\theta=14°$ suggest that the 154-meV feature is actually composed of three losses at 137, 154, and 173 meV. The losses at 82, 137, and 154 meV were observed in a preliminary study of this system, using a different EEL spectrometer.[29] Spectra taken at $\Delta\theta=28°$ support this deconvolution of the 154-meV feature and indicate the presence of an additional loss near 65 meV. The 65-meV loss is clearly visible in spectra taken at $\Delta\theta=14°$ and $E_i=4.50$ eV [Fig. 1(d)], as is a loss at 125 meV. The 125-meV loss may be present as a shoulder to the 137-meV loss in Fig. 1(c). There also is consistent intensity near 193 meV in all spectra taken under the conditions of Fig. 1(d). All losses exhibit substantial shifts in spectra taken of D-covered surfaces (see Fig. 2) and are attributed to motion of adsorbed hydrogen. The observed loss frequencies are presented in Table I. While appropriate selection of experimental conditions allows quantitative deconvolution of the 137- and 154-meV losses for H, the two losses always appeared as an unresolved feature at ≈104 meV in D spectra [see Fig. 2(b)].

Figure 3 displays the evolution of the HREEL spectra as a function of H coverage at $E_i=6.9$ eV; the loss energies are summarized in Table II. At the minimum coverage achievable, 0.32 ML [Fig. 3(d)], the 65- and 82-meV

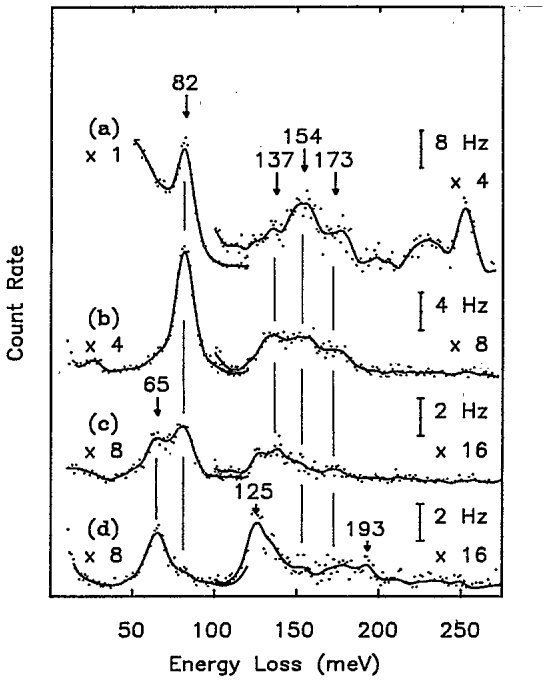

FIG. 1. HREEL spectra of 1.0 ML H adsorbed on Rh(100). Spectra (a)–(c) were taken at $E_i=5.85$ eV and the following $\Delta\theta$: (a) 0°, (b) 14°, and (c) 28°. Spectrum (d) was taken at $E_i=4.5$ eV and $\Delta\theta=14°$. The FWHM of the elastic beam was 9 meV in the four spectra. The elastic beam saturated the electron multiplier at $\Delta\theta=0°$.

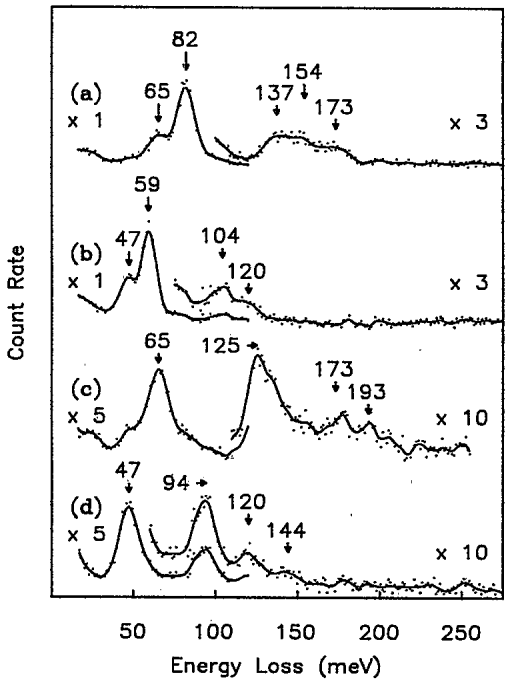

FIG. 2. Comparison of HREEL spectra of saturation H and D exposures to Rh(100). Spectra (a), H, and (b), D, were taken at $E_i=6.9$ eV and $\Delta\theta=14°$ and represent 55 min of data-acquisition time. Spectra (c), H, and (d), D, were taken at $E_i=4.5$ eV and $\Delta\theta=14°$; they are the average of a number of spectra. Spectrum (c) represents 138 min of data acquisition, while spectrum (d) represents 193 min of data acquisition.

TABLE I. HREELS results for saturation H and D coverages on Rh(100).

Assignment	H (meV)	D (meV)
ν_{asy}	65.5±0.5	47±1
ν_{sym}	82.0±0.3	59.2±0.3
overtones	125 ±2	94 ±1
	137 ±4	104[a]
	154 ±2	104[a]
	173 ±2	120 ±2
	193 ±2	144 ±1

[a]The 137- and 154-meV H-derived losses are unresolved on D-covered surfaces.

losses present at 1.0 ML are shifted to significantly lower energy, 50 and 70 meV, respectively. At this low coverage, no distinct higher-energy losses are observable at any E_i; however, the monotonically decreasing shoulder between 80 and 140 meV is a reproducible feature in the low-coverage spectra. At coverages intermediate between 0.32 and 1.0 ML [Figs. 3(b) and 3(c)] the spectra appear to consist of a superposition of low-coverage losses and 1.0-ML losses. This is similar to the behavior of H/Ni(100).[19] The large width of the transitions and their close spacing result in indistinct spectra at these intermediate coverages; however, the existence of a low-energy shoulder at 50 meV is a signature of the low-coverage component of the spectra.

All H-derived loss features were observed to be broader than the instrumental resolution at all E_i. At 1.0 ML and FWHM of the principal excitations, deconvoluting the instrumental resolution as the root difference of squares, are 10±2 meV for the 65-meV loss and 8±2 meV for the 82-meV loss (one-standard-deviation error bars). There was no detectable dependence of these linewidths on either the E_i or the isotope. The widths of the H-derived losses at higher energies (125–193 meV) could not be accurately determined; however, attempts to quantitatively fit the spectra indicate that these losses are broader than the two at 65 and 82 meV, with widths of order 16 meV. The width of the D-derived higher-energy losses appear visibly narrower than those of H. At

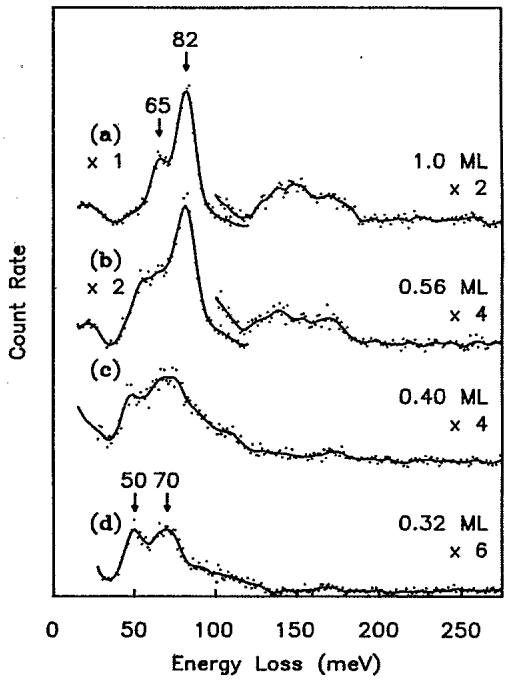

FIG. 3. HREEL spectra of H on Rh(100) as a function of coverage. E_i was 6.9 eV (correctly compensating for the coverage dependence of the H-induced change in the work function) and $\Delta\theta = 14°$. Spectra (a)–(c) represent 55 min of data acquisition. Spectrum (d) is the average of four spectra totaling 193 min of data acquisition.

$E_i = 4.5$ eV (see Fig. 2), the FWHM of the 94-, 120-, and 144-meV features are 13±1, 16±3, and 13±5 meV, respectively. Our lack of *a priori* knowledge of the widths of the losses above 100 meV prohibits accurate deconvolution of the spectra and is the principal source of uncertainty in the overtone loss energies. For examples, at $E_i > 5$ eV, where the 137-meV loss is flanked by the 154-meV loss and the 125-meV loss is weak, the best NLS fits to the spectra indicate that the peak is located near 134 meV; similarly, at $E_i < 4.5$ eV, where the 137-meV loss is flanked by the 125-meV loss and the 154-meV loss is

TABLE II. Vibrational losses of H (D) as a function of concentration and coverage.

	Rh(100)		Ni(100)	Pd(100)
Conditions	$\nu_{asy}^{0\to1}$ (meV)	$\nu_{sym}^{0\to1}$ (meV)	$\nu_{sym}^{0\to1}$ (meV)	$\nu_{sym}^{0\to1}$ (meV)
100% H (D) at 1 ML	65.0±0.3 (45.8±0.3)	82.4±0.4 (61.4±0.4)	78 (55)[a]	63.5 (45.2)[b]
0% limit H (D) at 1 ML	73.0±0.3 (50.9±0.3)	77.4±0.4 (55.4±0.4)	72 (51)	60.1 (42.7)
100% H at low coverage	49.9±0.4[c]	70±1[c]	66[d]	63.0[e]

[a]Reference 19.
[b]Reference 40.
[c]H coverage of 0.3 ML.
[d]H coverage was not reported; the H_2 exposure was 0.25 L vs 21 L for saturation coverage, Ref. 19.
[e]H coverage of 0.5 ML, Ref. 40.

weak, the best NLS fits indicate the peak is located near 140 meV. This is the source of the 3-meV error bar on this loss. The FWHM of the 50-meV loss at 0.32 ML is 10±2 meV, unchanged from the width at 1.0 ML. The FWHM of the 70-meV loss is greater than 20 meV, significantly broader than at 1.0 ML; however, the presence of some intensity at 82 meV in the low-coverage spectra would be unresolved and would bias our determination of the 70-meV loss width.

The angular dependence of the 82- and 154-meV losses at 1.0 ML coverage indicate that dipole scattering is contributing to their cross section and that the transitions are between vibrational states of A_1 symmetry. In spectra taken at 6-meV FWHM resolution, the elastic beam does not saturate the electron multiplier and the intensity of the 82-meV loss is found to be 0.0011 of the elastic. This can be contrasted with the normalized intensity of the dipole-active loss at 112 meV for H/Pt(111) (Ref. 30) of ≈ 0.0001 and with the normalized intensity of the dipole-active loss at 79 meV for H/Ni(110) (Ref. 31) of ≈ 0.0024. As the spectrometer is of a fixed-angle design, it is difficult to calibrate the angular acceptance and we forgo the calculation of an absolute dynamic dipole moment. The Pt and Ni studies were performed with the spectrometer utilized in this study, and the dynamic dipole moments of the H/Pt(111) and H/Ni(110) have been previously determined to be <0.009 (Ref. 32) and 0.03 (Ref. 33), respectively. Thus the dynamic dipole moment of H/Rh(100) can be estimated to be ≈ 0.02. The 82-meV loss is readily assigned to the fundamental excitation of the perpendicular vibration, ν_{sym}, of H in a fourfold hollow by analogy with previously characterized fcc (100) surfaces (see Table II) and theoretical calculations.[7–9,34,35] The 65-meV loss is assigned to the doubly-degenerate fundamental excitation of the parallel vibration, ν_{asy}. This is consistent with the E symmetry of the ν_{asy} since the loss at 65 meV exhibits no dipole character and is in excellent agreement with a recent LAPW calculations.[35]

The distinct H features at 125, 137, 154, 173, and 193 meV are first observed at coverages near 0.5 ML and their intensity is proportional to the intensity of the high-coverage fundamental transitions (65 and 82 meV). There are no distinct changes in the H_2 TDS for coverages below 0.8 ML;[29] TD spectra consist of a single symmetric peak characteristic of second-order desorption. Therefore, the losses above 100 meV are not due to a new binding site as it is unlikely that a separate H binding site would exhibit such a strong correlation to the 82-meV loss without having a substantial concentration and thus an observable signature in the TDS. We attribute these high-energy losses to overtones, and their assignment is postponed until the discussion (Sec. IV C).

In early HREELS studies, a nearest-neighbor central-force-constant (NNCFC) model was used to guide the interpretation of spectra.[1,36,37] In the NNCFC model the vibrational potential is represented by the harmonic approximation of a pairwise-additive central potential, restricted to nearest-neighbor interactions. For the threefold-hollow site appropriate to H adsorbed on the trigonal close-packed surfaces, and the fourfold-hollow site appropriate to H adsorbed on the fcc (100) surfaces, this potential predicts a simple relationship between the ν_{asy}, ν_{sym} and the adsorption geometry:

$$\frac{\nu_{asy}}{\nu_{sym}} = \frac{1}{\sqrt{2}} \tan\alpha \ , \tag{1}$$

where α is the angle between the H—M bond and the surface normal. LAPW calculations for H/Ru(001) (Ref. 5) and H/Pt(111) (Ref. 6) have indicated that Eq. (1) significantly overestimates the ratio $\nu_{asy}/\nu_{sym} \equiv \mathcal{R}$. This failure of the NNCFC model has been confirmed by a recent compilation of HREELS results for H bound in threefold-hollow sites.[30] However, the NNCFC model represents the vibrational potential of a twofold bridge site H/W(100) well. The W—H bond length derived from HREELS (Ref. 36) is 1.15±.05 Å, while dynamical LEED (Ref. 38) calculations obtain the value 1.17±.04 Å. The recent observation[20] of the ν_{asy} of 0.5 ML H on Pd(100) at 76 meV [contrast with the ν_{sym} of 63 meV (Ref. 20)] with our determination of the ν_{asy} for H/Rh(100) allow a test of the applicability of the NNCFC to fourfold-hollow sites. Neglecting any reconstruction of the surface layer [consistent with results from LEED (Refs. 26 and 27)], Eq. (1) predicts H-bonding radii (the difference between the M—H bond lengths and the M atomic radius) of 1.34 and 0.89 Å for 0.3 ML H/Rh(100) and 0.5 ML H/Pd(100), respectively. These values are clearly unphysical, as can be seen by comparison with the recent forward recoil scattering experiments, which have determined the values 0.56 Å for H/Ni(100) (Ref. 39) and 0.63 Å for H/Pd(100) (Ref. 28), and *ab initio* calculations, which have obtained values of 0.58 Å H/Pd(100) (Ref. 9) and 0.64 Å for H/Rh(100) (Ref. 35). If we compare the experimental $\mathcal{R}$ and Rh and Pd with those computed from Eq. (1) based on the theoretically calculated binding geometries,[9,35] we find that the NNCFC model overestimates $\mathcal{R}$ by a factor of 3 for Rh and 6 for Pd. This is in sharp contrast with H in the threefold-hollow site, where, although the NNCFC model incorrectly predicted the ratio of frequencies, the error in $\mathcal{R}$ was only a factor of 1.4.[30] It is clear that extreme caution must be exercised in the application of the NNCFC model to highly (3 or 4) coordinated H.

B. Isotopic dilutions

The significant coverage-dependent shift in the H loss energies (both fundamentals shift by at least 12 meV) can arise due to both static changes in the vibrational potential and dynamic coupling between the H. The dynamic contribution can be measured by studying H-D isotopic mixtures as was originally done by Nyberg and Tengstål.[40] The mass difference is sufficient that the H and D oscillators are dynamically uncoupled, yet, within the Born-Oppenheimer approximation, they experience the same static potential. Figure 4 shows spectra of dilute D in a H-saturated surface and dilute H in a D-saturated surface taken at E_i of 6.1 eV (optimal for observation of ν_{sym}) and 4.5 eV (optimal for observation of ν_{asy}). Figure 5 displays the concentration dependence of the fundamental excitations of both isotopes. The uncer-

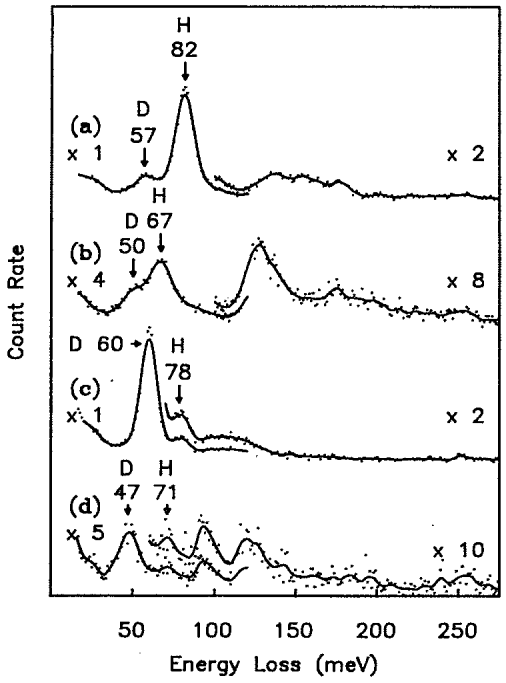

FIG. 4. HREEL spectra of H and D mixtures, 1.0 ML total coverage. Spectra (a) and (b) were taken of a mixture containing 18% D. Spectrum (a) was recorded at $E_i = 6.1$ eV and $\Delta\theta = 8°$, while spectrum (b) was recorded at $E_i = 4.5$ eV and $\Delta\theta = 14°$. Spectrum (c) is of a 75% D mixture, taken under the same conditions as spectrum (a). Spectrum (d) is of a 62% D mixture, taken under the same conditions as spectrum (b). All four spectra are the average of multiple runs, totaling a minimum of 110 min.

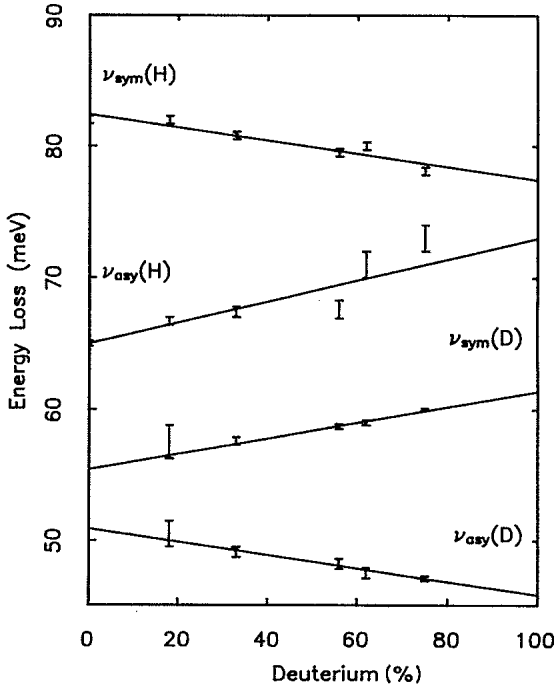

FIG. 5. Dependence of the loss frequencies for the fundamental transitions on the relative concentration of D at saturation total coverage. The lines are weighted least-squares fits to the data; the 0% and 100% limits of the fits are presented in Table II.

tainties in the frequencies were determined by inversion of the curvature matrix[41] from the NLS fit to spectra which were the average of typically four independently prepared H (D) mixtures. The dilution shifts of the overtones could not be determined accurately. It is observed that the ν_{sym} of the dilute species is lower than that of the full ML, while the ν_{asy} of the dilute species is higher than that of the full ML. The total shift in the frequency between the full ML and dilute systems is of the order of 5 meV for both ν_{sym} and ν_{asy}. Table II summarizes the results of the dilution experiments by reporting the full ML and 0% extrapolations of linear fits to the concentration dependence of the frequencies.

C. Impact-energy dependence

The E_i dependence of the loss intensities is interesting and proved crucial to the study of the overtone losses. As has been observed in a number of systems,[13,20,37] the H loss intensities are intimately related to the surface reflectivity, which is shown in the inset to Fig. 6. The transmission function of the spectrometer for a given tuning is constant over approximately a 2-eV range in E_i; thus the reflectivity was determined by mapping a series of E_i segments and splicing them together. This does not affect the location of sharp extrema, but subtle, slow vari-

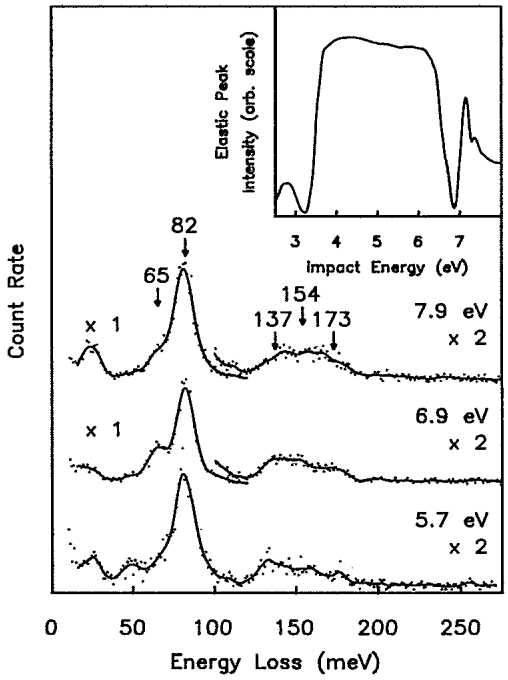

FIG. 6. HREEL spectra of 1.0 ML H on Rh(100) taken at E_i near 7 eV with $\Delta\theta = 14°$. The inset displays the E_i dependence of the intensity of the specularly scattering elastic beam for an H-covered surface.

ations in the reflectivity may be obscured. The transmission of the spectrometer decreases at low E_i, so the drop in reflected current below 4 eV may be due in part to the instrument response. Between 4.1 and 6.1 eV the reflectivity of the H-saturated surface is very bright (exceeding that of the clean surface) and relatively featureless. The two sharp minima at 6.90 and 7.40 eV are attributed to image-potential states associated with the emergence of the first LEED beam at 7.6 eV. The cause of the minimum at 3.2 eV is uncertain. The adsorption of H significantly affects the reflectivity of Rh(100) at low E_i, and the minimum at 3.2 eV may be due to a surface resonance (in the language of McRae[42]) arising from a H-induced surface-electronic state. In their study of H/Pd(100), Conrad *et al.*[20] observed a minimum in the specular reflectivity of H-saturated surfaces at low E_i (near 1.5 eV) and attributed the feature to a H-induced surface state.

Figure 6 displays spectra taken at $\Delta\theta=14°$ and E_i near 7 eV, where the image-potential-state resonances occur in the specular reflectivity. Spectra at $E_i=7.9$ and 5.7 eV are typical at most E_i between 5.3 eV and the maximum E_i characterized, 7.9 eV. The ν_{sym} is the dominant feature, with the three losses at 137, 154, and 173 meV all exhibiting comparable intensity. The feature at low loss energy (25 meV) observed at $E_i=7.9$ and 5.7 eV did not shift with substitution of D or H and is assigned to a substrate surface phonon or resonance. Near 6.9 eV, the ν_{asy} exhibits resonancelike enhancement; however, the intensity of the ν_{asy} does not reach that of the ν_{sym}. The 125-meV loss is not clearly observed above 5 eV. The intensities of all losses measured at $\Delta\theta=14°$ exhibit a pronounced minimum at $E_i\approx5.3$ eV. The high specular reflectivity of the sample at E_i near 5 eV indicates the absence of many diffuse scattering channels and is consistent with the weak, large-angle inelastic-scattering intensity.

Figure 7 summarizes a series of HREELS spectra taken with E_i near the specular reflectivity minimum at 3.2 eV. All losses exhibit a resonancelike enhancement, peaking near $E_i=3.8$ eV. The diffusely scattered elastic intensity, at $\Delta\theta=14°$, exhibits a maximum at $E_i=4.0$ eV. This maximum in diffuse scattering is associated with the minimum in specular scattering at $E_i=3.2$ eV. The difference between the energy of the diffuse scattering maximum (4.0 eV) and the specular reflectivity minimum (3.2 eV) arises from the resonance condition on the incident parallel momentum, and the 7° decrease in the incident angle associated with the 14° increase in the scattering angle. The H-derived losses do not exhibit a maximum in intensity at precisely the same E_i as the diffuse elastic intensity. Specifically, the fundamental transitions at 65 and 82 meV exhibit a maximum at $E_i=3.8$ eV and the losses at 137 and 154 meV exhibit a maximum at $E_i=3.9$ eV, while the losses at 125 and 173 meV exhibit a maximum at $E_i=4.0$ eV. More intriguing is the observation that the intensities of the losses decrease at significantly different rates as E_i is increased above 3.7 eV. This effect is most prominent in spectra taken near $E_i=4.5$ eV, where the ν_{asy} and the 125-meV

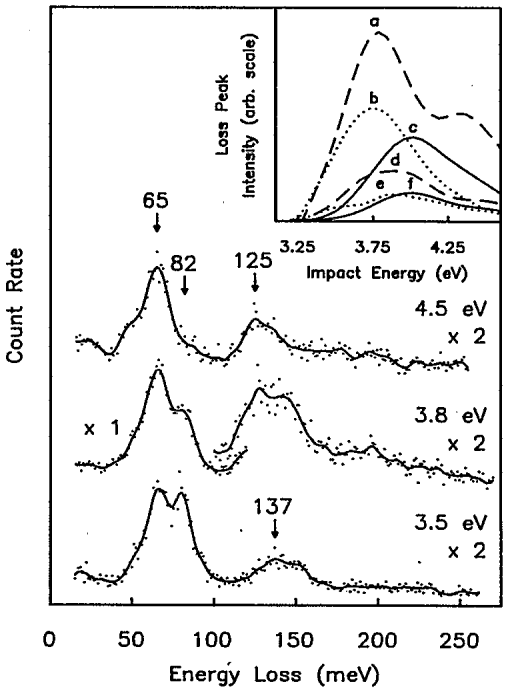

FIG. 7. HREEL spectra of 1.0 ML H on Rh(100) taken at E_i near 4 eV with $\Delta\theta=14°$. The inset displays the intensity of the principal loss peaks at $\Delta\theta=14°$ for E_i between 3.3 and 4.5 eV. The key is *a* (— — —), 65 meV; *b* (·····), 82 meV, *c* (——), 125 meV; *d* (— — —), 137 meV; *e* (·····), 154 meV; *f* (——), 173 meV.

loss dominate the spectra [see Fig. 7(a)]. The marked contrast between spectra taken at $E_i=4.5$ and 6.1 eV was crucial in performing the isotope-dilution experiments, as it allowed spectra essentially containing only two of the four closely spaced fundamental transitions (ν_{asy}, ν_{sym} for both H and D) to be obtained.

In a previous study of H/Pd(111) and H/Pd(100),[20] it was noted that the inelastic cross sections exhibited the most dramatic enhancement at E_i near the H-induced surface states and that the enhancement appeared to be mode selective. The ν_{asy} was more intense than the ν_{sym} when E_i was close to the H-induced surface state, yet ν_{sym} was more intense than ν_{asym} when E_i was near the image-state resonances. The behavior of H/Rh(100) is similar, assuming the reflectivity minimum near 3.2 eV is correctly attributed to an H-induced surface site. Unfortunately, there presently exists no theoretical explanation for the apparent dependence of the inelastic cross section on the polarization of the vibration and the nature of the surface resonance. The experimental correlation does suggest that the 125- and 193-meV H-derived losses, prominent at low E_i (see Figs. 2 and 7), may be due to motion predominantly parallel to the surface. Accurate calculations of the E_i dependence of the inelastic cross section for scattering from the ν_{sym} and ν_{asy} of H/W(100) have recently been performed[43] and have established the breakdown of pseudoselection rules for specular scattering when E_i is near image-state resonances. There is a

clear need for comparable calculations under conditions where all transitions are allowed to establish the utility of using E_i studies to aid in the determination of mode polarizations.

IV. DISCUSSION

A. Fundamental transitions: Evidence for adsorbate-adsorbate interaction

The assignment of the fundamental transitions is straightforward and was made in the preceding section. The distinction between ν_{sym} and ν_{asy} is unambiguous due to the significant dipole cross section of the ν_{sym}. The substantial changes in the HREEL spectra with coverage indicate that the vibrational potential is very sensitive to H-H interactions. On both the Rh(100) and Ni(100) surfaces, spectra of intermediate coverages appear to consist of the superposition of well-defined low- and high-coverage losses. On Pd(100), H forms an ordered $c(2\times2)$ structure at 0.5 ML, and nucleates ordered islands at low temperature.[44] This is manifest in the EELS as spectra of the $c(2\times2)$ structure exhibit a single narrow ν_{sym} at 63.0 meV.[40] The ν_{sym} appears at 63.5 meV for the (1×1) saturated surface. The presence of $c(2\times2)$ islands implies the surface will consist of only two local densities as a function of coverage: 0.5 ML with no nearest neighbors (NN's) and 1.0 ML with four NN's. This obviously would lead to HREEL spectra with a distinct superposition of losses at coverages above 0.5 ML if H-H interactions substantially affected the vibrational potential. The appearance of significant amounts of the high-coverage species at 0.56 ML on Rh(100) [Fig. 3(b)] indicates that large, well-ordered $c(2\times2)$ domains are not present on Rh(100), consistent with the absence of any detectable fractional order spots in LEED.[27] [Random addition of atoms to a well-ordered $c(2\times2)$ surface at 0.5 ML would result in 12% of the H in (1×1) domains and 88% in $c(2\times2)$ domains at 0.56 ML total coverage.] However, it is intuitive to propose that H adsorbs with a short-ranged $c(2\times2)$ order, minimizing the number of NN contacts, as the vibrational spectra show evidence for a lateral repulsion. The coverage evolution of the EEL spectra would still be dominated by no NN species and four NN species, but the disorder would inhomogeneously broaden the distinct lines and lower the onset coverage for appearance of the four-NN losses. The data in Fig. 3 do not allow a quantitative determination of the local adsorbate density, but are consistent with the assignment of the 50- and 70-meV losses to H with no or one NN and the 65- and 82-meV losses with H with three or four NN's. It is interesting to speculate on the correlation between distinctly observed overtone transitions and 1 ML local coverage. Site-to-site tunneling at dilue local coverage could broaden the vibrational levels near the top of the diffusion barrier (the overtones) sufficient to produce the indistinct shoulder present in 0.3-ML spectra.[45,46] The localization due to NN repulsion at (1×1) local coverage could produce more distinct overtones, while providing an additional source of parallel anharmonicity.

The substantial change in the fundamental frequencies as the number of NN's is increased could arise from static changes in the H binding potential from H-H interactions. The heat of adsorption of H on many of the group-VIII metals has been determined by both equilibrium measurements and TDS.[47] The binding energy is typically constant at low coverages and then decreases above some critical coverage. This is generally interpreted in terms of destabilizing H-H interactions. TDS of H/Rh(100) suggests that the H binding energy decreases at coverages above 0.8 ML.[29] The stiffening of the ν_{asy} of H surrounded by nearest neighbors is consistent with a H-H repulsion which could lead to destabilization. However, it is counterintuitive to observe such a dramatic *increase* in ν_{sym} as the binding energy *decreases*.

The discrepancy between the coverage dependence of the ν_{sym} and expectations based on the coverage dependence of the binding energy of H leads us to explore the significance of dynamic coupling in the full monolayer. The study of isotopically mixed layers, at fixed total coverage, allow a separation of dynamic and static effects. Isotope-dilution experiments for $^{12}C\,^{16}O/^{12}C\,^{18}O$ mixtures on a number of surfaces[2] have established the importance of direct dipole-dipole coupling in interpreting the vibrational spectra of CO. Isotope-dilution experiments for H/D mixtures on Pd(100) and Ni(100) have established the presence of a substrate-method electronic coupling of the ν_{sym}.[19,40] For the case of H (D) dilutions the masses are sufficiently different that the experiments have a simple interpretation. The isotopically pure H ML, assuming harmonic oscillators with linear coupling, has a set of adsorbate phonon branches as the normal modes. Under the conditions of the present experiments, $E_i \approx 5$ eV, $\Delta\theta \approx 14°$, the parallel momentum transfer, $\Delta q_{\parallel}$, associated with the scattering event is small, only 12% of the wave vector at $\bar{X}$. The EEL spectra, even off specular, essentially determine the zone-center ($\bar{\Gamma}$) phonon energy. For the case of dilute H in a saturated D layer, the large difference in vibrational frequencies implies that the D provides an essentially stationary environment for the H vibrations. An isolated mass defect (mass M_i) in a lattice is a textbook problem,[48] and the frequency of the localized vibration, Ω, taking into account the weakly correlated motions of the host (mass M_h), is given by the eigenvalue equation

$$\int \frac{g(\omega)d\omega}{\Omega^2-\omega^2} = \frac{1}{\epsilon\Omega^2} , \tag{2}$$

where $g(\omega)$ is the density of states, normalized to unity, of the host lattice, and $\epsilon=(M_h-M_i)/M_h$. For the case of the optic modes of the adsorbed hydrogen lattice, where ϵ is large, the dilute H loss will lie approximately in the center of the phonon band of the pure-H surface. The frequency shift between the dilute- and pure-isotope cases is thus approximately half the full width of the pure isotope band. The dilute-limit frequency, Ω, for H will generally be pushed slightly above the band center due to "repulsion" from the D states at lower frequency; similarly, Ω for D will be pushed slightly below the band center by the H states. Nordlander and Holmström,[49]

have explored the explicit concentration dependence of the ν_{sym} frequencies within the average T-matrix approximation (ATA) and obtained the result

$$(\omega_\alpha)^2=(\Omega_\alpha)^2+\frac{C_\alpha\phi_{int}}{M_\alpha}\ , \qquad (3)$$

where α labels the isotope (H or D), M is the isotope mass, C the isotope concentration, and ϕ_{int} is the mean vibrational interaction. For $\phi_{int}/M_\alpha\Omega_\alpha^2$ small, Eq. (3) leads to a linear dependence of the observed frequencies, ω, with concentration. The ν_{asy} will exhibit a similar concentration dependence, but with a different ϕ_{int}. Equations (2) and (3) are consistent, as the mean vibrational interaction determines the phonon bandwidth; however, Eq. (2) gives a more precise determination of Ω.

The results of weighted-least-squares fits of the data for ν_{asy} and ν_{sym} as a function of concentration in Fig. 5 give total frequency shifts (pure layer—dilute limit, in meV/ML) of -8 ± 1 (-5 ± 1) for H (D) ν_{asy}, and 5 ± 1 (6 ± 1) for the ν_{sym}. The 0% and 100% relative concentration limits of the best fits are presented in Table II. The ATA treatment predicts the total frequency shift should scale as $1/\sqrt{M}$, which is correct in the limit that the host atoms are rigid. The total observed shift for the ν_{sym} is essentially mass independent. This may be indicative of small systematic errors in the determination of the loss frequencies. However, from the qualitative discussion of Eq. (2) it is clear that the corrections due to the weakly correlated host motions will result in deviations from a strict $1/\sqrt{M}$ mass dependence. For the ν_{sym} the ratio of the total dilution shift of H and D will be $<\sqrt{2}$ since the dilute H loss is pushed "up," decreasing the measured shift, while the dilue D loss is pushed "down," increasing the shift. Similarly, the ν_{asy} should exhibit a ratio $>\sqrt{2}$.

The magnitude of the dilution shift for the ν_{sym} is comparable to the shifts measured on Ni(100) and Pd(100) (see Table II). This shift is much greater than can be attributed to either direct dipole-dipole interaction (the dynamic dipole moment for the ν_{sym} is small) or substrate-mediated mechanical coupling (the H is too light compared to the Rh lattice).[40] Direct overlap of the H wave functions (chemical bonding) is usually excluded on the grounds that the H-H separation is large compared with the bonding radius of H. Thus the coupling in the ν_{sym} has been attributed to a substate-mediated electronic interaction. Recently, the expected dilution shifts in the ν_{sym} of H on both Ni(100) and Pd(100) have been calculated with the effective-medium theory (EMT).[49] The magnitude and sign of the predicted shifts are consistent with the Ni and Pd data, as with this experiment. The increase in the ν_{sym} for the pure ML compared to the dilute ν_{sym} arises from H competition for the finite electron density of the metal. Since the metal electron density decreases exponentially with increasing vertical displacement into the vacuum, the H-H destabilization is more effective in pure monolayer, when the H are uniformly displaced from the surface, than in the dilute limit, since the increased metal electron density around the "static" neighbors "left behind" in the dilute case screens the interaction. Similarly, the observed dilution shift in the ν_{asy} cannot be attributed to direct dipole-dipole interactions as the sign of the shift, for parallel oriented dipoles, is of the opposite sign.[50] The rms displacement in the first parallel excited state (estimated from the frequency and the assumption of a harmonic oscillator) is appreciable (≈0.3 Å) but insufficient for direct overlap to be relevant. Therefore, the principal coupling mechanism for the ν_{asy} is also attributed to a substrate-mediated electronic interaction. The EMT calculations[49] noted some "localization" of H due to lateral interactions at 1.0 ML coverage; however, the magnitude of the calculated increase in ν_{asy} is substantially smaller than observed.

The full width of the hydrogen phonon bands are estimated by assuming a simple density of states (a rectangle of full width 2Δ, centered on ω_0) and fitting the dilute-limit frequency Ω calculated from Eq. (2) and the $\bar{\Gamma}$ phonon frequency ($\omega_0\pm\Delta$ depending on the sign of dispersion) to the data. Averaging the results for H and D (appropriately scaled), we obtain a full width of the H ν_{sym} phonon band of ~12 meV and a full width of the H ν_{asy} band of ~15 meV. Both the width of the ν_{sym} band (12 meV) and the sign of the dispersion away from the adsorbate Brillouin zone center (negative) are in accord with a recent EELS study of β_1-H/W(100),[51] where, by recording spectra at higher E_i and for very large scattering angles, the actual dispersion of the H phonons was measured. The W(100)-substrate Brillouin zone is larger than that of the 2-ML H overlayer; the overlayer zone-boundary ν_{sym} phonon is folded back to the zone center and is readily observed. The ν_{sym} disperses down from 130 meV at $\bar{\Gamma}$ to 124 meV at the substrate zone boundary and to 118 meV back at $\bar{\Gamma}$, giving a full width of the phonon band of 12 meV in the extended, adsorbate Brillouin zone.

The observation that ν_{asy} becomes stiffer in the dilute limit is again consistent with a H-H lateral repulsion. The magnitude of the ν_{asy} coupling is slightly larger than that of the ν_{sym}; this is in contrast to β_1-H/W(100),[51] where the dispersion of the in-plane modes was less than that of the ν_{sym}. Isotope-dilution spectroscopy has been performed for H/D mixtures on both Raney Ni (Ref. 52) and Pt black[53] using INS. In INS from polycrystalline samples, the scattering is from phonons of all wave vectors and the magnitude of the dilution shift is not directly comparable to that observed in EELS. In particular, since EELS provides data at $\bar{\Gamma}$ for the pure overlayer, the EELS experiment provides both an estimate of the bandwidth and the sign of the dispersion away from the zone center. INS experiments provide information on the magnitude of the bandwidth, but do not provide direct information on the sign of the dispersion. A recent HREEL study[30] has assigned the ν_{asy} of H/Pt(111) to a loss at 67 meV; a broad feature at 66 meV in INS spectra of H-saturated Pt black significantly narrowed and shifted to 73 meV for 10% H in a D-saturated sample.[53] The estimated bandwidth was ≈30 meV, indicating that substantial dispersion in both ν_{sym} and ν_{asy} is not uncommon.

In an attempt to further characterize the nature of the substrate-mediated electronic interaction between the H,

we performed additional experiments on 1 ML of H with deliberately coadsorbed CO. The coadsorption of H and CO on Rh(100) has been extensively characterized.[23,26,27] A saturation exposure of CO to the (1×1) H monolayer at 90 K produces an intimately mixed surface structure with all H remaining in the fourfold hollow and 0.5 ML of CO, bound to the top site, in a $c(2\times2)$ structure. The ν_{sym} of the H appears at 72.0±0.3 meV, significantly shifted from the 82-meV value in the absence of CO. The ν_{asy} is not observed as the very strong Rh-CO frustrated vertical translation at 56 meV interferes. During TDS, 0.5 ML of H will desorb as H_2 in an approximately zeroth-order desorption peak near 150 K, substantially below the second-order desorption peak temperature at 320 K characteristic of H in the absence of CO. In a previous report, the decrease in ν_{sym} was correlated to the decrease in the H binding energy apparent in the TDS.[27] We have seen that the ν_{sym} frequency does not clearly reflect the coverage-dependent changes in the H binding energy in the absence of CO. Since the observed frequency for the coadsorbed system (72 meV) is approximately the low-coverage frequency in the absence of H-H interaction, we performed dilution experiments to determine if the principal effect of the CO on the H vibrational levels was simply a screening of the H-H interaction. The ν_{sym} of H in a CO-on-(H+D) coadsorbed system containing 59% D appears at 69.5±0.4 meV, indicating that the dynamic coupling in the coadsorbed system is comparable to that in the absence of CO. (The H ν_{sym} of a surface containing a 62% D mixture appears at 80.0±0.3 meV, compared to the 0% D value of 82.0±0.3 meV; to within experimental accuracy, the H dilution shift at 60% D in the presence of CO, 2.5±0.6 meV, and in its absence, 2.0±0.4 meV, are identical.) The substantial decrease in the binding energy of the H in the presence of CO is thus associated with a real softening of the average potential for perpendicular displacements. The observation that the highly polarizable CO molecule did not significantly affect the dynamic coupling provides additional evidence that the coupling is not due to dipole-dipole interactions. It is interesting that the perturbations in the H-metal bonding induced by the strongly chemisorbed CO do not alter the substrate-mediated coupling. The similarity in the ν_{sym} bandwidth for saturation H coverages on the four surfaces Ni(100),[19] Pd(100),[40] Rh(100), and W(100),[51] the insensitivity of the magnitude of the coupling to the presence of strongly interacting coadsorbed CO, and the substantial bandwidths evident for the ν_{asy} on Rh(100) and Pt(111) (Ref. 53) suggest that dynamic coupling is a general phenomena in H vibrational levels.

B. Model of coupled anharmonic oscillators

We now turn our attention to the observed transitions to higher-lying vibrationally excited states within the full monolayer of H. The study of these excitations involves the interplay of two effects: (1) anharmonicity of the single-site potential, and (2) dispersion caused by coupling forces between hydrogen atoms. Since the bandwidth of the dispersion (10–16 meV) is of the same order as the measured anharmonic shifts, clearly a description solely using isolated H oscillators is not appropriate to the analysis of the overtone frequency shifts.

We can see this most clearly by using a simple 1D model of coupled anharmonic oscillators to study the interplay between anharmonicity and coupling. The results of this model will be used to guide a qualitative discussion of the EELS data. While the corresponding quantitative model of 3D vibrations of hydrogen in a 2D monolayer would be feasible numerically, a purely phenomenological fit would involve more parameters than we have measured quantities. Either more detailed experimental dispersion relations and better-resolved overtones, or a total-energy calculation, will be necessary before quantitative fits will make sense.

The model Hamiltonian is that of a one-dimensional chain of N anharmonic oscillators with a linear coupling:

$$\mathcal{H}=\sum_{m}^{N}\frac{p_m^2}{2M}+(\tfrac{1}{2}M\omega_0^2u_m^2+au_m^3+bu_m^4)-Ku_mu_{m+1}\ , \tag{4}$$

where u_m is the displacement away from equilibrium of the atom at lattice site m (the lattice spacing is unity), p_m is the conjugate momentum, K is the interatomic force constant, ω_0 is the small-oscillation frequency of a single H atom with the other atoms fixed in position, and a and b parametrize the local anharmonic site potential.

This Hamiltonian has been used frequently in studies of the anharmonicity and cooperative vibrational excitations in molecular solids, usually using Green's-function methods. Two-phonon bound states have been discussed by Kimball *et al.*[54] with a model almost identical to ours; the optical-absorption intensity has been calculated by Holstein *et al.*[55] In the context of surface science and electron-energy-loss spectroscopy, Ariyasu and Mills[56] have developed a sophisticated and complete Green's-function analysis of the model using approximations equivalent to ours. None of the results presented in this section are new. Our approach of explicitly calculating the energy eigenstates does, however, illuminate some features of this problem in a new light.

There are two natural starting points for studying this system: starting from localized oscillators and starting from plane waves. In the localized oscillator basis, the single-site Hamiltonian

$$\begin{aligned}\mathcal{H}^{\rm loc}&=\frac{p^2}{2M}+\tfrac{1}{2}M\omega_0^2u^2+au^3+bu^4+\cdots\\&=\sum_{n=0}^{\infty}E_n\,|\,E_n\rangle\langle E_n\,|\end{aligned} \tag{5}$$

has excited state energies $E_0,E_1,E_2,\ldots$ whose spacings are shifted from the harmonic value $\hbar\omega_0$. The interatomic coupling $\mathcal{H}^{\rm coup}=\mathcal{H}-\mathcal{H}^{\rm loc}=-K\sum_m u_mu_{m+1}$ can then be expanded in this basis. In particular, the expansion of the displacement u_m of the mth adsorbed atom in the localized oscillator basis has the general form

$$u=\sum_{i,j}u_{ij}\,|\,E_i\rangle\langle E_j\,|\ . \tag{6}$$

In the plane-wave basis, we diagonalize the harmonic part of the Hamiltonian by going to normal modes $\tilde{u}_k=(1/\sqrt{N})\sum_m u_m e^{ikm}$:

$$\mathcal{H}^{\text{harm}}=\sum_m \frac{p_m^2}{2M}+\tfrac{1}{2}M\omega_0^2 u_m^2-Ku_m u_{m+1}$$
$$=\sum_{k=-\pi/a}^{\pi/a}\frac{\tilde{p}_k^2}{2M}+\tfrac{1}{2}M\omega_k^2\tilde{u}_k^2 \ . \tag{7}$$

The coupling between the adsorbed atoms gives the dispersion relation

$$\omega_k=[\omega_0^2-(2K/M)\cos(k)]^{1/2}$$
$$=\omega_0-(K/M\omega_0)\cos(k)+O(K^2/M^2\omega_0^3) \ . \tag{8}$$

The anharmonic terms $\mathcal{H}^{\text{anharm}}=\mathcal{H}-\mathcal{H}^{\text{harm}}=\sum_m au_m^3+bu_m^4$ appear perturbatively as phonon-phonon scattering. We will see, however, that the anharmonic terms have significant nonperturbative effects.

We will solve this problem numerically, with two approximations. (1) We assume $\hbar\omega_0$ is large. Since, experimentally $\hbar\omega_0\approx 70$ meV is large compared either to the anharmonicity $2E_1-E_2\approx 10$ meV or to the bandwidth $2\hbar K/M\omega_0\approx 10$–$15$ meV, this allows us to work within the subspaces of fixed number n of total excitations (e.g., with energies roughly $n\hbar\omega_0$ above the ground state). (2) We incorporate the anharmonicity [a and b in Eq. (4)] solely through shifting the energies E_n within a given anharmonic well. The eigenstates, of course, also are changed by the anharmonicity. These come into the calculation only through the expansion of u in $\mathcal{H}^{\text{coup}}$ [Eq. (6)]. We will use the harmonic form for u,

$$u=\left[\frac{\hbar}{2M\omega_0}\right]^{1/2}(a^\dagger+a) \ . \tag{9}$$

The harmonic form for the expansion of u throws away no physics relevant to the discussion in this section (and avoids introducing undetermined parameters); however, a proper calculation of excitation cross sections, selection rules, or isotope shifts would demand a more complete calculation.

In the subspace of single excitations (the one-excitation sector), within approximation (2) above, the local oscillator states are

$$|\,m\,\rangle=a_m^\dagger\,|\,\psi_0\rangle \ ,$$

Here, ψ_0 is the (unexcited) ground state, and the $|\,m\,\rangle$ are eigenstates of $\mathcal{H}^{\text{loc}}$ with energy E_1. The coupling term

$$\mathcal{H}^{\text{coup}}=-(\hbar K/2M\omega_0)\sum_l (a_l^\dagger+a_l)(a_{l+1}^\dagger+a_{l+1}) \tag{10}$$

leads, within the one-excitation sector, to the truncated $N\times N$ Hamiltonian

$$\mathcal{H}=\mathcal{H}^{\text{loc}}+\mathcal{H}^{\text{coup}}=\begin{bmatrix} E_1 & -\hbar K/2M\omega_0 & 0 & \cdots & 0 & -\hbar K/2M\omega_0 \\ -\hbar K/2M\omega_0 & E_1 & -\hbar K/2M\omega_0 & \cdots & & \\ \vdots & \vdots & & & & \vdots \\ -\hbar K/2M\omega_0 & 0 & \cdots & & -\hbar K/2M\omega_0 & E_1 \end{bmatrix} . \tag{11}$$

The eigenstates naturally are plane waves $|\,k\,\rangle=1/\sqrt{N}\sum_m e^{ikm}\,|\,m\,\rangle$ with energies $E_k=E_1-\hbar K/M\omega_0\cos(k)$, which agrees with Eq. (8) to terms of order $\hbar K^2/M^2\omega_0^3$.

In the two-excitation sector, the local oscillator states are given by

$$|\,l,m\,\rangle=\begin{cases} a_l^\dagger a_m^\dagger\,|\,\psi_0\rangle, & l>m \\ (1/\sqrt{2})a_l^\dagger a_l^\dagger\,|\,\psi_0\rangle, & l=m \ . \end{cases}$$

The states $|\,l,m\,\rangle$ and $|\,m,l\,\rangle$ are indistinguishable: each has the two sites singly excited. The $\sqrt{2}$ is necessary to normalize the doubly excited overtone state. Thus the truncated Hamiltonian is of size $[N(N+1)/2]\times[N(N-1)/2]$. $\mathcal{H}^{\text{loc}}$ is diagonal in this basis, with eigenvalues $2E_1+(E_2-2E_1)\delta_{lm}$. The off-diagonal terms of the Hamiltonian in this basis are

$$\langle l',m'\,|\,\mathcal{H}^{\text{coup}}\,|\,l,m\,\rangle=-\frac{\hbar K}{2M\omega_0}(\sqrt{2})^{-(\delta_{lm}+\delta_{l'm'})}\langle\psi_0\,|\,a_{l'}a_{m'}\sum_n (a_n^\dagger a_n)(a_{n+1}^\dagger+a_{n+1})a_l^\dagger a_m^\dagger\,|\,\psi_0\rangle$$
$$=-\frac{\hbar K}{2M\omega_0}(\sqrt{2})^{-(\delta_{lm}+\delta_{l'm'})}\langle\psi_0\,|\,a_{l'}a_{m'}(a_{l+1}^\dagger a_m^\dagger+a_{l-1}^\dagger a_m^\dagger+a_l^\dagger a_{m-1}^\dagger+a_l^\dagger a_{m+1}^\dagger)\,|\,\psi_0\rangle \ .$$

Since by convention $l\geq m$,

$$\langle l',m'\,|\,\mathcal{H}\,|\,l,m\,\rangle=[2E_1+(E_2-2E_1)\delta_{lm}]\delta_{ll'}\delta_{mm'}$$
$$-(\hbar K/2M\omega_0)(\sqrt{2})^{\delta_{l'm'}+\delta_{lm}}[(\delta_{l',l+1}+\delta_{l',l-1})\delta_{m'm}+\delta_{ll'}(\delta_{m',m-1}+\delta_{m',m+1})] \ .$$

This is the Hamiltonian in the two-excitation sector in the local oscillator basis.

We can gain some insight into this truncated Hamiltonian by taking some limits. In the limit $E_2=2E_1$ one may check that the eigenstates are products of two plane waves; if the wave vectors are k and k', the energy is

$$E_k+E_{k'}=2E_1-(\hbar K/M\omega_0)(\cos k+\cos k') .$$

In the uncoupled limit $K=0$ there is an $[N(N-1)/2]$-fold-degenerate space of energy $2E_1$ (two excitations on distinct sites) and an N-fold-degenerate space of energy E_2 (the double-excited overtone on a single site). When $K\neq 0$, the states at $2E_1$ form the two-phonon band, even when $E_2\neq 2E_1$; the energy levels and wave functions thereof differ from the sum of two one-phonon excitations only by contributions of order $1/N$. The overtone states with a single atom in the second-excited state are of most interest to us. These become a band of excitations near E_2 when the coupling is introduced.

The total crystal momentum $\hbar k_0$ remains a good quantum number in our system. By using the plane-wave basis, we can work at fixed k_0 and reduce the size of our matrices by a factor of N. In the two-excitation sector we define the plane-wave basis

$$|k,k'\rangle=\begin{cases}\dfrac{1}{N}\displaystyle\sum_l\sum_m e^{ikl}e^{ik'm}a_l^\dagger a_m^\dagger|\psi_0\rangle, & k\neq k'\\ \dfrac{1}{\sqrt{2}N}\displaystyle\sum_l\sum_m e^{ik(l+m)}a_l^\dagger a_m^\dagger|\psi_0\rangle, & k=k' .\end{cases}$$

We split $\mathcal{H}=\mathcal{H}^{\text{harm}}+\mathcal{H}^{\text{anharm}}$, where

$$\mathcal{H}^{\text{harm}}|k,k_0-k\rangle=(E_k+E_{k_0-k})|k,k_0-k\rangle$$

and

$$\mathcal{H}^{\text{anharm}}|l,m\rangle=(E_2-2E_1)\delta_{lm}|l,m\rangle .$$

One can then show that the plane-wave matrix elements of $\mathcal{H}^{\text{anharm}}$ are

$$\langle k',k_0-k'|\mathcal{H}^{\text{anharm}}|k,k_0-k\rangle=(1/N)(\sqrt{2})^{2-\delta_{k',k_0-k'}-\delta_{k,k_0-k}}(E_2-2E_1) .$$

Consider for the moment the energy spectrum for a harmonic crystal with a fixed total crystal momentum k_0. In the plane-wave basis, the system has an energy eigenstate with total energy E_{tot} above the ground state if there is a set of n phonons whose energy sums to E_{tot} and whose wave vectors sum to k_0. Since the phonon spectrum spans a narrow range around $\hbar\omega_0$, the complete excitation spectrum consists of narrow ranges of energies centered on multiples of this frequency. The lowest of these ranges gives the one-phonon dispersion relation; above this lies a two-phonon band which for fixed k_0 ranges over all energies $E_{\text{tot}}=\hbar\omega_k+\hbar\omega_{k_0-k}$, and so forth.

Figure 8 shows the one- and two-excitation sectors of $\mathcal{H}$ in Eq. (4), within the approximations noted above.

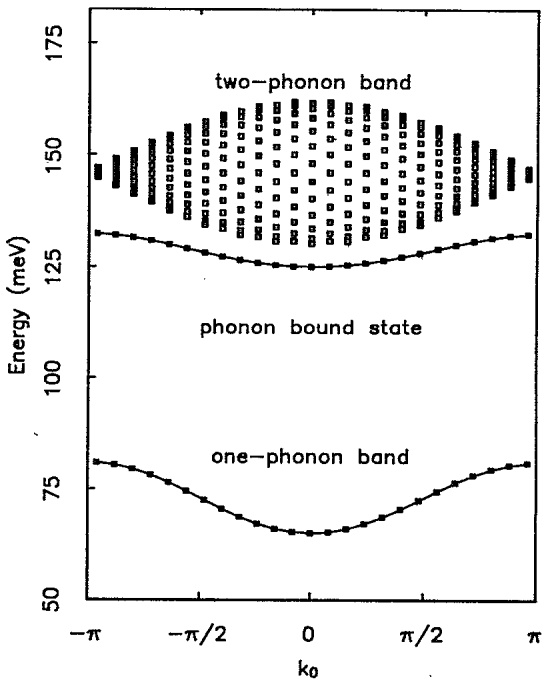

FIG. 8. Results of the model calculation of a chain of linearly coupled, anharmonic, 1D oscillators. The band of states centered at 73 and 146 meV are the familiar one- and two-phonon bands. The band centered at 128 meV is a two-excitation bound state associated with the anharmonic overtone of the uncoupled oscillators.

The parameters $E_1=73$ meV and $\hbar K/M\omega_0=8$ meV were chosen to reproduce the observed dispersion of the ν_{asy} band; the parameter $E_2=132.4$ meV was then chosen to reproduce the zone-center frequency of the "overtone" at 125 meV. One observes the one- and two-phonon bands as expected from the harmonic theory.

In addition, one sees a new excitation split off from the two-phonon band. It has a natural interpretation in the localized basis. Imagine freezing all the atoms at their equilibrium positions except one, and exciting that atom into the anharmonic, second-excited state $|E_2\rangle$ of the frozen-neighbor potential. We now unfreeze the neighbors, and allow them to respond to the motion of the excited atom. If the anharmonicity is large enough, the excited atom cannot efficiently couple to its neighbors. In particular, if the anharmonic vibration frequency is outside of the allowed two-phonon excitations, it is in the stop band of the lattice and produces an exponentially decaying response. It is a bound state of two vibrational excitations. Explicitly, an eigenstate in the two-excitation sector with wave vector k_0 is of the form

$$\psi(l,m)\equiv\langle l,m|E_s(k_0)\rangle=e^{ik_0(l+m)/2}\psi_{k_0,s}(l-m) , \quad (12)$$

where the index s distinguishes the N states consistent with each k_0. Figure 9 shows the $k_0=0$ wave function $\psi_0(l-m)$ for the bound state.[57] Most of the amplitude has the two excitations on the same site $l=m$. The mixing between the isolated overtone and the two-phonon

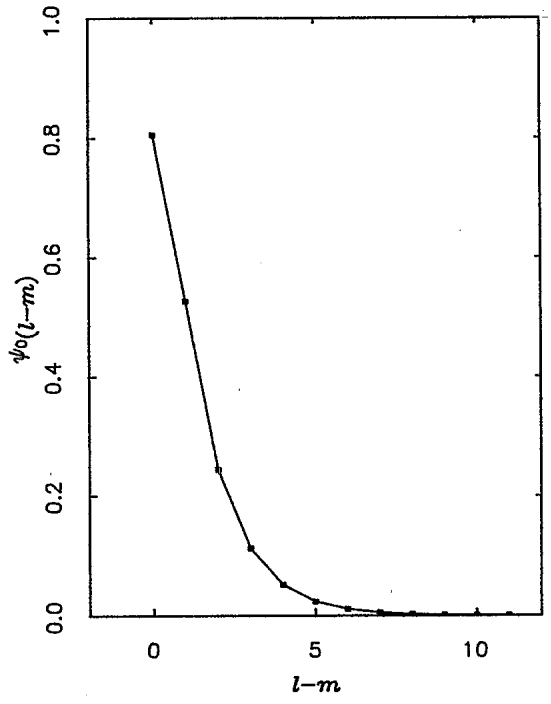

FIG. 9. The $k_0=0$ wave function for the two-excitation bound state associated with the anharmonic overtone of the uncoupled oscillators. The wave function is only defined for $l-m>0$.

band produces the tails in the wave function and is also the source (within the harmonic form for u) for the dispersion of the bound state. At the zone center, the local mode is close to the two-phonon band and is pushed down in energy, while at the zone boundary the levels are farther apart and the interaction is weaker.

We need more than the energy spectrum to interpret an experiment: we need to know how our probe couples to the various states. (See Ref. 56 for a more systematic approach to this problem.) For dipole scattering, the differential cross section $d^2\sigma/d\Omega\, d\hbar\omega$ can be related to the thermal fluctuations in the charge density[58] in a manner similar to the Van Hove formulation for inelastic neutron scattering as

$$\frac{d^2\sigma}{d\Omega\, d\hbar\omega}=\frac{32m^2e^2\pi^3}{\hbar^2\cos\alpha}\frac{k'}{k}\left|\left\langle\psi_{\mathbf{k}'}^{-}\left|\frac{z}{|\mathbf{x}|^3}\right|\psi_{\mathbf{k}}^{+}\right\rangle\right|^2 S(\mathbf{q},\omega)\ , \tag{13}$$

where $\psi_{\mathbf{k}}^{+}$ and $\psi_{\mathbf{k}'}^{-}$ are in- and out-going electron-scattering wave functions with wave vectors $\mathbf{k}$ and $\mathbf{k}'$; α is the angle of incidence, $d\Omega$ is the differential solid angle, and $\mathbf{q}=\mathbf{k}_{\parallel}-\mathbf{k}'_{\parallel}$ is the parallel momentum transfer. The spectral function for the dipole-dipole correlation function is defined as

$$S(\mathbf{q},\omega)=\int\frac{dt}{2\pi}e^{i\omega t}\frac{1}{N}\sum_{l,m}e^{i\mathbf{q}\cdot(\mathbf{R}_l-\mathbf{R}_m)}\langle\mu(\mathbf{R}_l,t)\mu(\mathbf{R}_m,0)\rangle_T\ , \tag{14}$$

where $\mu(\mathbf{R}_l,t)$ is the normal component of the time-dependent dipole moment of the atom located at $\mathbf{R}_l$ and $\langle\ \rangle_T$ is a thermal average. The generalization of Eqs. (13) and (14) to higher-order multipole scattering is obvious. Since the spectra were recorded at $k_BT\ll E_1$, we will replace the thermal average with the ground-state expectation value. In order to calculate the correlation function, the time-dependent dipole moment is expanded in the displacement of each atom away from equilibrium,

$$\mu(\mathbf{R}_l,t)=\mu^0(\mathbf{R}_l)+\sum_{\alpha}e_{\alpha}^{*1}(\mathbf{R}_l)u_{\alpha}(\mathbf{R}_l,t)+\sum_{\alpha,\beta}e_{\alpha\beta}^{*2}(\mathbf{R}_l)u_{\alpha}(\mathbf{R}_l,t)u_{\beta}(\mathbf{R}_l,t)+\cdots\ , \tag{15}$$

where α,β are Cartesian coordinates, e_{α}^{*1} is the linear effective charge vector, $\partial\mu(\mathbf{R}_l)/\partial u(\mathbf{R}_l)$, $e_{\alpha\beta}^{*2}$ is the quadratic effective charge tensor, and we have neglected crossterms such as $\partial\mu(\mathbf{R}_l)/\partial u(\mathbf{R}_m)$, $l\neq m$. Since in our model we have kept the harmonic wave functions and introduced anharmonicity only through the energy eigenvalues, the first term in the dipole moment expansion that couples to the two-excitation sector is the quadratic effective charge tensor.[59] Thus we concentrate our attention on the expectation value (and simplify the notation for one dimension, $l\equiv\mathbf{R}_l$)

$$\langle\psi_0\,|\,u(l,t)u(l,t)u(m,0)u(m,0)\,|\,\psi_0\rangle\ .$$

Inserting Eq. (6) for $u(l,t)$, the only term that produces inelastic transitions is (neglecting all arithmetic factors)

$$\langle\psi_0\,|\,a_l(t)a_l(t)a_m^{\dagger}(0)a_m^{\dagger}(0)\,|\,\psi_0\rangle\ .$$

This can be evaluated by inserting a complete set of two-excitation-sector states $|E_s(k_0)\rangle\langle E_s(k_0)|$ and shifting the time evolution from the destruction operators onto the states to give

$$\sum_{k_0,s}\langle ll\,|\,E_s(k_0)\rangle e^{-i\omega(k_0,s)t}\langle E_s(k_0)\,|\,mm\rangle\ .$$

Inserting the local basis Bloch form of $|E_s(k_0)\rangle$ from Eq. (12), we have

$$S(q,\omega)\propto\int\frac{dt}{2\pi}e^{i\omega t}\frac{1}{N}\sum_{l,m}e^{iq(l-m)}\sum_{k_0,s}\psi(0)_{k_0,s}\frac{e^{-ik_0l}}{\sqrt{N}}e^{-i\omega(k_0,s)t}\frac{e^{ik_0m}}{\sqrt{N}}\psi(0)_{k_0,s}\ . \tag{16}$$

The time integral will produce an energy-conservation δ function, while the lattice sum will produce a wave-vector-conservation δ function. Thus at fixed momentum transfer q, the differential cross section will be determined by

$$\sum_s |\psi(0)_{q,s}|^2 \delta(\omega-\omega(k_0,s)) , \tag{17}$$

which is the density of states projected onto the double excitation of a single site and is shown for $q=0$ in Fig. 10. Clearly, for scattering via the quadratic effective charge, coupling to the bound state is much larger than to the unbound pairs of phonons. In a more realistic treatment of the model Hamiltonian, the cubic anharmonicity will cause mixing between the two-excitation sector and the one- and three-excitation sectors. The one-excitation-sector component will allow coupling to the two-excitation sector by the linear effective charge. This will still favor excitation of the bound state since the anharmonic terms in the two-phonon state (which in the thermodynamic limit are the simple sum of two one-phonon states) are smaller than in the bound state (which closely resembles the localized oscillator overtone), as confirmed by the calculations of Holstein *et al.*[55] Finally, what will happen for smaller values of the anharmonicity? Generally, if the anharmonicity $2E_1-E_2$ is smaller than the dispersion, the isolated overtone will oscillate in the passband of the two-phonon states, and we expect that the excitation will have a finite lifetime. The bound state becomes a resonance, and the projected density of states will broaden (but probably will be peaked near the overtone energy, rather than centered on the two-phonon band). Only near wave vectors where the passband is particularly narrow (π and $-\pi$ in Fig. 8) will the bound state survive. Unfortunately, the one-dimensional model here fails us: no matter how small the anharmonicity, it never has a resonance. (An arbitrarily small coupling produces a bound state in one-dimensional quantum mechanics.) Two- and three-dimensional calculations with both model[54-56,60] and realistic[61] phonon densities of states have been published.

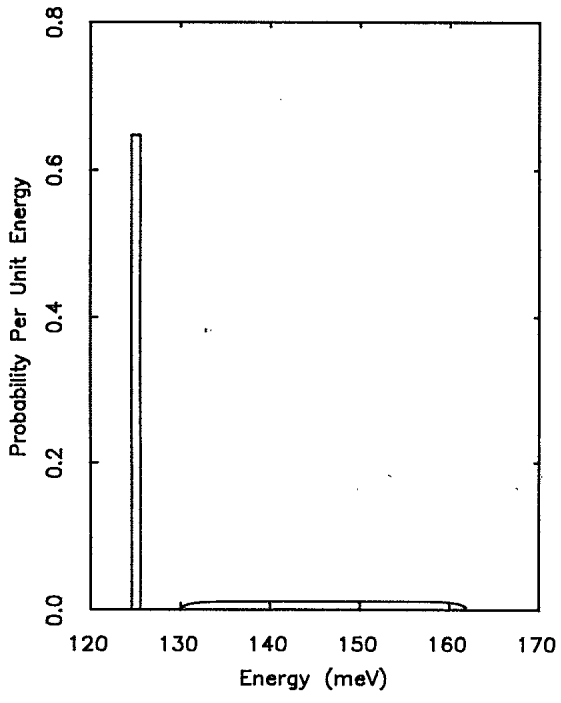

FIG. 10. Density of states in the two-excitation sector projected onto double excitation of a single site. This projected density of states determines the EELS differential cross section for transitions into the sector via the quadratic effective charge.

C. The overtone spectra

In the past the effects of dynamic coupling have been ignored in the interpretation of overtone spectra. In a recent study of H/Ru(001), all three principal losses corresponding to the ν_{asy} overtone ($\nu_{asy}^{0\to2}$), $\nu_{asy}^{0\to1}+\nu_{sym}^{0\to1}$ combination mode, and the ν_{sym} overtone ($\nu_{sym}^{0\to2}$), were observed.[14] Although the ν_{asy} shifted from 86 to 102 meV as a function of coverage, indicating H-H interactions are important, a simple 2D potential was constructed to describe the vibrational well of uncoupled H oscillators, and the anharmonic terms were estimated from a fit of the data to a first-order perturbation treatment of the potential. The model gives rise to energy levels given by

$$E=\hbar\omega_z(n_z+\tfrac{1}{2})+\hbar\omega_x(n_x+\tfrac{1}{2})+B_0+B_z(n_z+\tfrac{1}{2})^2 +B_{zx}(n_z+\tfrac{1}{2})(n_x+\tfrac{1}{2})+B_x(n_x+\tfrac{1}{2})^2 , \tag{18}$$

where ω_z and ω_x are the harmonic frequencies and the B's are readily calculated from the potential. The five observed H frequencies determined the values $\hbar\omega_x=118$, $\hbar\omega_z=146$, $B_x=-6$, $B_{zx}=-8$, and $B_z=-0.5$ meV. The anharmonic terms indicate significant parallel anharmonicity and parallel-vertical coupling; however, the strictly perpendicular curvature, determined by B_z, is quite harmonic. The anharmonicity of the potential was actually used to assign the inelastic transitions; the most anharmonic fundamental was attributed to the ν_{asy} parallel mode. The same logic (association of the most anharmonic fundamental, based on the observed overtone frequencies, to the ν_{asy}) has been used to assign the HREELS spectra of H/Pd(111). A naive comparison of the observed "overtones" for H/Rh(100) with Eq. (18) would result in the assignment of the 125-meV loss to the $\nu_{asy}^{0\to2}$, the 137-meV loss to the $\nu_{asy}^{0\to1}+\nu_{sym}^{0\to1}$, combination mode, the 154-meV loss to the $\nu_{sym}^{0\to2}$, and 173-meV loss to the $\nu_{asy}^{0\to3}$. The weak loss at 193 meV could be the $\nu_{asy}^{0\to2}+\nu_{sym}^{0\to1}$ combination mode. The six principal H losses and the three D losses ($\nu_{asy}^{0\to1}$, $\nu_{sym}^{0\to1}$, $\nu_{asy}^{0\to2}$) are consistent (with 1.2-meV root-mean-square deviation) with the values $\hbar\omega_x=77.2$, $\hbar\omega_z=95.5$, $B_x=-3.6$, $B_{zx}=-9.5$, and $B_z=-4.6$ meV, producing the counterintuitive result that the perpendicular curvature is more anharmonic than the parallel curvature. However, neglect of the dispersion of the transition in the analysis can lead to substantial errors, since the HREELS spectra correspond to approximately constant-k energy scans,

near $k=0$. Consider the case of harmonic phonons; the HREEL spectra will consist of a narrow one-phonon loss and a broad feature due to the two-phonon band. If the analysis did not account for the linear coupling, the two losses would be readily assigned to a fundamental excitation at $\omega(k_0=0)$ and a broad overtone at $2\omega(k_0=0)+\Delta$, where Δ is $\frac{1}{2}$ the full one-phonon bandwidth. Thus the coupled harmonic system would appear as *a strongly anharmonic isolated oscillator.*

The same error in attribution of dispersion related frequency shifts to anharmonicity can be made for the two-excitation bound state (Fig. 8) arising from the anharmonic overtone. Since the dispersion of the bound state is less than that of the one-phonon band; the loss energies measured at the zone center underestimate the local site anharmonicity. In particular, the $k=0$ HREELS spectrum of Fig. 8, approximated by Fig. 10, would indicate that the overtone energy E_2 (125 meV) is 5 meV below the harmonic value $2E_1$ (2×65 meV), while, in reality, E_2 (132.4 meV) is 13.6 meV below the harmonic value $2E_1$ (2×73 meV). We expect the dispersion-induced errors in the estimation of the anharmonicity of resonance levels to be similar, although we do not have a quantitative model of the dispersion of the resonance losses.

It is clear that, in general, the presence of coupling distorts the estimates of anharmonicity from HREEL spectra at fixed $\Delta q_{\parallel}$. The two-excitation bound states, due to anharmonicity, are weakly coupled to their neighbors, and thus exhibit less dispersion than the one-phonon band. The greater the site anharmonicity, the weaker the coupling and the narrower the bound-state band. Experimentally, this could be treated by studying the dilute-limit spectra of isotopically mixed system; when the coupling is minimized, however, the weak intensity of the overtones usually prohibit such a procedure. (In this study, the overtones could not be measured at relative concentrations below 50%. As the uncertainty in their position, due to their substantial widths, was large, no conclusions could be drawn concerning their dilution shift.) It should be noted that the accidental near degeneracy of the 124-meV H overtone and the 120-meV D overtone could result in unusual dilution shifts in those losses.

Using the 1D model to guide our analysis, we present a qualitative discussion of the overtone spectra. The observed HREELS data for the two fundamentals and the four lowest-lying overtones are summarized in Fig. 11, along with estimates of the two-phonon band positions. The 2D nature of the Brillouin zone is neglected for clarity. The ν_{asy} and ν_{sym} one-phonon bands are determined from the isotope-dilution experiments. We have chosen to depict the three possible combinations of phonon polarizations in the two-phonon bands separately to facilitate correlation of the data with the overtones and combination modes of the isolated oscillator. It is clear that the 125- and 173-meV losses are outside the multiphonon

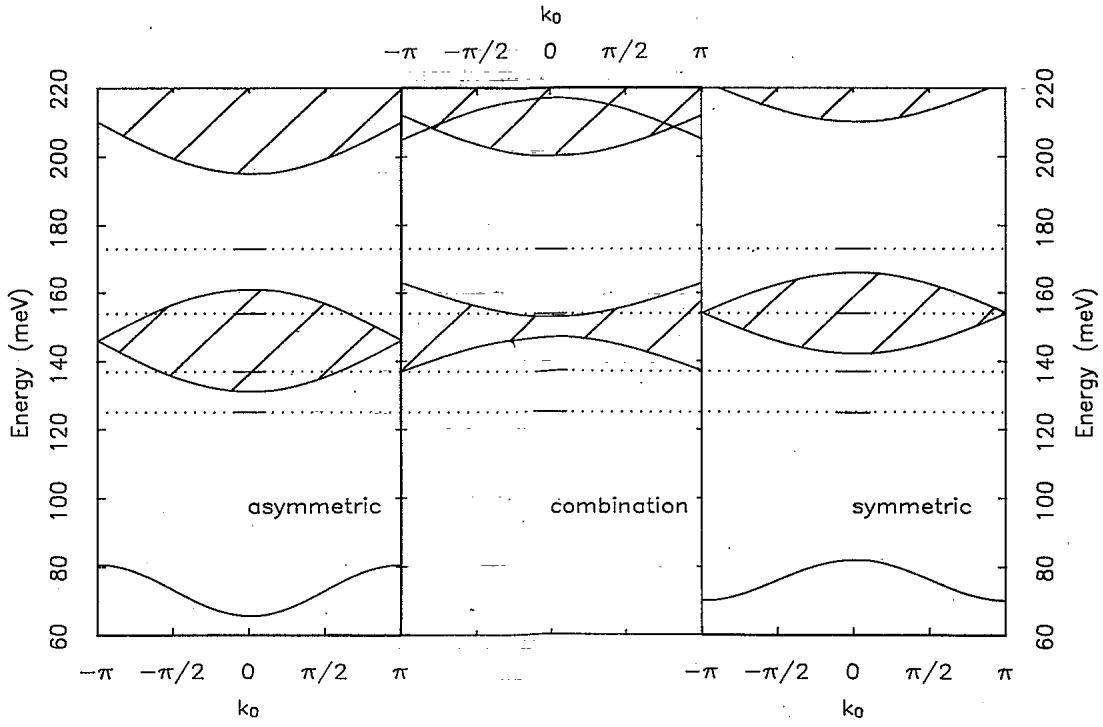

FIG. 11. Schematic diagram of the observed overtone transitions for 1.0 ML H on Rh(100) and their relationship to the phonon bands estimated from the isotope-dilution experiments. The horizontal lines indicate the experimental overtone losses at $k_0\approx0$. The solid lines are $\cos(k_0)$ representations of the one-phonon bands; the $k_0=0$ energy and the full width were determined from the isotope dilutions. The shaded regions are the two-phonon bands, obtained from representative one-phonon dispersion curves.

bands, and correspond to localized bound states, while the 154- and 137-meV losses fall within the two-phonon bands and are resonances. As the resonances and bound states can be correlated with the overtones of the uncoupled oscillator, we present a brief discussion of the symmetries of the excited states of the local potential. This discussion will be applicable to the phonon symmetries at the high-symmetry points of the Brillouin zone, $\bar{\Gamma}$ and $\bar{M}$. The C_{4v} symmetry of the fourfold-hollow site implies that the representation carried by the normal modes is A_1+E, which readily relates to the $\nu_{\rm sym}$ (A_1) and doubly degenerate $\nu_{\rm asy}(E)$. All the excited states of the A_1 normal mode are of A_1 symmetry; however, care must be taken in the calculation of the symmetry of the overtones of the doubly-degenerate E normal modes.[62] The second-excited state of the $\nu_{\rm asy}$ carries the representation $A_1+B_1+B_2$, while the third-excited state carries the representation $2E$. The $\nu_{\rm sym}+\nu_{\rm asy}$ combination band carry the representation of the simple product of the two components and thus the symmetry is determined by the $\nu_{\rm asy}$ component. Note that the introduction of anharmonicity can completely lift the degeneracy of the $\nu_{\rm asy}$ overtones.

From Fig. 11 it is clear that the most natural assignment of the 125-meV loss is to a $\nu_{\rm asy}^{0\to2}$ two-phonon bound state as was assumed in the 1D model. This is supported by the E_i dependence of the cross section, since the 125-meV loss intensity correlated with the intensity of the parallel polarized $\nu_{\rm asy}$. From the previous discussion it is clear that the 5-meV shift between twice the zone-center one-phonon loss and the two-phonon bound state underestimates the effect of anharmonicity on the parallel oscillations. The large anharmonicity observed for the $\nu_{\rm asy}^{0\to2}$ suggests that the 173-meV loss could arise from one of the E-symmetry $\nu_{\rm asy}^{0\to3}$. If so, it is so far below the three-phonon band that it is effectively uncoupled.

The assignment of the 137-meV loss is not at all clear. It could correlate to a $\nu_{\rm asy}^{0\to1}+\nu_{\rm sym}^{0\to1}$ resonance well below the two-phonon combination band, as was suggested by the simple 2D independent-oscillator model, or the loss could be due to a $\nu_{\rm asy}^{0\to2}$ resonance, since a correct 3D model of the independent oscillator allows the $\nu_{\rm asy}^{0\to2}$ to be split into three nondegenerate modes. The E_i dependence of the loss suggests it has some perpendicular character as the loss is most easily observed at energies above 5 eV, where the $\nu_{\rm sym}$ is the dominant spectral feature. This does not resolve the issue, as the anharmonicity can introduce perpendicular character into the $\nu_{\rm asy}^{0\to2}$. It is interesting to note that, since the $\nu_{\rm sym}$ and $\nu_{\rm asy}$ have comparable dispersions with opposite sign, the simple sum $\nu_{\rm asy}^{0\to1}+\nu_{\rm sym}^{0\to1}$ observed at $\bar{\Gamma}$ is a good approximation of the location of the harmonic two-phonon combination band.

The 154-meV loss is most naturally attributed to the $\nu_{\rm sym}^{0\to2}$ resonance. This is consistent with the E_i dependence of the loss as it is most readily characterized at high E_i, and with the observed dipole activity. If the dynamic dipole is only linear in coordinate displacement, the $\nu_{\rm sym}^{0\to2}$ transition can only be excited by coupling to the anharmonic components of the resonance. The shift in the frequency of the resonance away from the isolated overtone will depend on the details of the density of states of the two-phonon band, and quantitative discussion of the anharmonicity is problematic. We expect the dispersion of the resonance to be less than the dispersion of the one-phonon band, so that comparison of zone-center frequencies for the $\nu_{\rm sym}^{0\to1}$ one-phonon loss and the $\nu_{\rm sym}^{0\to2}$ two-phonon resonance will overestimate the anharmonicity of the excitation. Since we tend to overestimate the vertical anharmonicity and underestimate the parallel anharmonicity, the nonintuitive conclusion, based on the 2D uncoupled model calculation, that the vertical potential is more anharmonic than the parallel potential is probably incorrect.

Recently, the internal bond energy of CO adsorbed on clean and potassium-precovered Ru(001) has been estimated from the anharmonicity of the CO intermolecular stretch and the Birge-Sponer extrapolation.[63,64] An anharmonic shift $(2\omega_{\rm CO}^{0\to1}-\omega_{\rm CO}^{0\to2})$ of 4.3 meV was measured for 0.33 ML CO on the clean surface, while a substantially greater shift of 23.6 meV was measured for the severely red-shifted $\omega_{\rm CO}$ present after a 0.25-L exposure of CO to a surface covered with 0.10 ML K. The 4.7-meV increase in $\omega_{\rm CO}^{0\to1}$ between 0 and 0.33 ML coverage observed on the clean surface can be accounted for by dynamic coupling between the CO time-dependent dipole moments.[65] The dynamic coupling between CO's produces a dispersion similar to that of the $\nu_{\rm sym}$ of H/Rh(100), and the 4.3-meV shift in the $\bar{\Gamma}$ transition energies overestimates the anharmonicity of the CO oscillator. Thus the estimate of the bond dissociation energy for the adsorbed species of 7.4 eV (contrast with the gas-phase value of 11 eV) is a lower bound on the true dissociation energy (assuming the Birge-Sponer extrapolation is accurate). The red-shifted $\omega_{\rm CO}$ in the presence of K exhibits a dramatic (174→196 meV) increase as a function of CO coverage, attributed to a substrate-mediated electronic interaction in direct analogy with the $\nu_{\rm sym}$ of H/Rh(100). Once again, the 23.6-meV shift in the $\bar{\Gamma}$ transition energy will overestimate the anharmonicity of the CO oscillator.

The most certain of our tentative assignments is that of the 125-meV loss to a $\nu_{\rm asy}^{0\to2}$ derived two-phonon bound state. Based on the 1D model, the overtone level, in the absence of H-H coupling, would be at least 10 meV below the harmonic value of $2\nu_{\rm asy}^{0\to1}$. The conclusion that the parallel vibrations are highly anharmonic appears to be contradicted by the observation that the isotope shift of the $\nu_{\rm sym}^{0\to1}$ (comparing the 100% H value of 65.5 meV to the 100% D limiting of 45.8 meV) is 1.43, slightly greater than $\sqrt{2}$. Qualitatively, one expects the D to sample a more restricted region of the potential than the H; thus the D should exhibit smaller deviations from the harmonic potential. If the potential is soft, so that the H frequencies of the overtones are less than twice the fundamental, the isotope shift should be smaller than $\sqrt{2}$. However, this qualitative picture has limited utility when applied to 2D and 3D oscillators. For example, in the 2D model [Eq. (18)] of the uncoupled oscillators, the B parameters scale inversely as the adsorbate mass $(1/M)$ in the frozen-substrate limit, while the harmonic frequencies

vary as $1/\sqrt{M}$. This gives rise to deviations from the classical $\sqrt{2}$ mass shift. However, both B_{zx} and B_x determine the $\nu_{\text{asy}}^{0\to1}$ frequency, while only B_x determines the displacement of $\nu_{\text{asy}}^{0\to2}$ from $2\nu_{\text{asy}}^{0\to1}$. Therefore, if the two correction terms have opposite sign, the isotope shift will be small, but the frequency shift of the overtone can be large. The frequency shifts of the one-phonon band due to anharmonicity can be calculated in perturbation theory, if the dynamical matrix is known.[66] The result is qualitatively similar to the preceding discussion; the anharmonic frequencies $\omega(k)$ are the sum of the harmonic $\omega(k)$ and a correction $B(k)$ which varies as $1/M$. $B(k)$ is a complicated combination of the coefficients of the anharmonic terms in the potential and thus can be ≈ 0 if the anharmonic terms enter with different signs.

A similar discussion is required by the observation that the 154-meV loss, tentatively assigned to a $\nu_{\text{sym}}^{0\to2}$ resonance, indicates the ν_{sym} is harmonic, yet the ν_{sym} shows an isotope shift of 1.34. In the terms of the 2D uncoupled model, this is quite naturally explained by a large, negative B_{zx} with a small B_z. This agrees with the earlier concept of attributing the major anharmonicities to the parallel motion. Note that a large negative B_{zx} will place the combination band below the harmonic estimate $\nu_{\text{asy}}^{0\to1}+\nu_{\text{sym}}^{0\to1}$, consistent with the observed location of the 137-meV loss. However, a large negative B_{zx} and a large negative B_x are inconsistent with the 2D uncoupled model and the small deviation of isotope shift of the $\nu_{\text{asy}}^{0\to1}$ from $\sqrt{2}$. For a 3D, doubly-degenerate oscillator appropriate to the fourfold-hollow site, the expression for the energy of a level [Eq. (18)] contains two additional terms, $B_{xy}(n_x+\frac{1}{2})(n_y+\frac{1}{2})$ and a more complicated term which lifts the degeneracy of the A_1 and B_1 linear combination of the $n_{x \text{ or } y}=2$, $n_{y \text{ or } x}=0$ harmonic overtones.[67] Thus it is still possible to have a $\sqrt{2}$ isotope shift for the $\nu_{\text{asy}}^{0\to1}$ and a large, negative shift of the $\nu_{\text{asy}}^{0\to2}$; however, one of the in-plane coupling terms must be large and positive.

Hamann and Feibelman[35] have calculated the anharmonicity of the H/Rh(100) potential using local-density-functional theory and the LAPW method. In order to fully utilize the symmetry of the overlayer, they calculated the energy of the system for uniform displacements of all the H ($q=0$ "frozen phonons") and fit an effective 3D single-particle potential to the results. Their variational solutions for the first-excited states should accurately model the $q=0$ one-phonon transitions observed by EELS. However, their solutions for the higher excited states will not be as accurate since the displacements in the two-phonon bound state are localized to only a few lattice sites. The calculations indicate that the parallel potential is very anharmonic, in agreement with experiment.

V. CONCLUSIONS

We have presented the results of the first complete study of the vibrational spectra of adsorbed H in which both the local site anharmonicity and dynamic coupling between the oscillators are treated. The mode-specific resonant enhancement of the inelastic transitions at select impact energies was instrumental in the successful performance of the experiments. The fundamental transitions establish that H is adsorbed in the fourfold-hollow site at all coverages. As is the case for the threefold-hollow site of hcp (001) (Ref. 5 and 14) and fcc (111) surfaces,[6,30] the NNCFC model is in substantial quantitative disagreement with the observed frequencies. The coverage dependence of the ν_{sym} vibration does not reflect the coverage variation of the binding energy; the observed frequency shift instead reflect substantial dynamic coupling between the H.

The presence of the dynamic coupling complicates the interpretation of the overtone transitions observed at high coverage. A 1D model of coupled anharmonic oscillators establishes that dynamic coupling can result in substantial errors in the interpretation of overtone spectra. Guided by the qualitative insight provided from the model, we are able to establish that the dominant anharmonicity is in the x-y plane. The model also suggests that dynamic coupling will cause the recent estimates of CO intermolecular bond energies from the observed anharmonicity to be systematically weak. As dynamic coupling appears to be ubiquitous to many adsorbate systems, it is clear that quantitative models of the dispersions of both the fundamental and overtone transitions are required for complete understanding of the vibrational spectra.

ACKNOWLEDGMENTS

Support for this research was provided by the National Science Foundation under Grant No. DMR-84-13561.

*Present address: Surface Science Division, National Institute for Standards and Technology, Gaithersburg, MD 20899.

[1]H. Ibach and D. L. Mills, *Electron Energy Loss Spectroscopy and Surface Vibrations* (Academic, New York, 1982).
[2]F. M. Hoffmann, Surf. Sci. Rep. **3**, 107 (1983).
[3]R. F. Willis, A. A. Lucas, and G. D. Mahan, in *Chemical Physics of Solid Surfaces and Heterogeneous Catalysis,* edited by D. A. King and D. P. Woodruff (Elsevier, New York, 1983), Vol. 2, Chap. 2.
[4]R. Biswas and D. R. Hamann, Phys. Rev. Lett. **56**, 2291 (1986).
[5]P. J. Feibelman and D. R. Hamann, Surf. Sci. **179**, 153 (1987).
[6]P. J. Feibelman and D. R. Hamann, Surf. Sci. **182**, 411 (1987).
[7]C. Umrigar and J. W. Wilkins, Phys. Rev. Lett. **54**, 1551 (1985).
[8]M. Weinert and J. W. Davenport, Phys. Rev. Lett. **54**, 1547 (1985).
[9]D. Tománek, S. G. Louie, and C.-T. Chan, Phys. Rev. Lett. **57**, 2594 (1986).
[10]M. Y. Chou and J. R. Chelikowsky, Phys. Rev. Lett. **59**, 1737 (1987).
[11]W. Eberhardt, S. G. Louie, and E. W. Plummer, Phys. Rev. B **28**, 465 (1983).
[12]P. J. Feibelman, D. R. Hamann, and F. J. Himpsel, Phys. Rev. B **22**, 1734 (1980).

[13]W. Ho, R. F. Willis, and E. W. Plummer, Phys. Rev. Lett. **40**, 1463 (1978); Phys. Rev. B **21**, 4202 (1980).
[14]H. Conrad, R. Scala, W. Stenzel, and R. Unwin, J. Chem. Phys. **81**, 6371 (1984).
[15]H. Conrad, M. E. Kordesch, R. Scala, and W. Stenzel, J. Electron. Spectrosc. Relat. Phenom. **38**, 289 (1986).
[16]J. J. Rush, J. M. Rowe, and D. Richter, Z. Phys. B **55**, 283 (1984).
[17]J. Eckert, J. A. Goldstone, D. Tonks, and D. Richter, Phys. Rev. B **27**, 1980 (1983).
[18]H.-J. Tao, K.-M. Ho, and X.-Y. Zhu, Phys. Rev. B **34**, 8394 (1986).
[19]P.-A. Karlsson, A.-S. Mårtensson, S. Andersson, and P. Nordlander, Surf. Sci. **175**, L759 (1986).
[20]H. Conrad, M. E. Kordesch, W. Stenzel, M. Šunjić, and B. Trninic-Radja, Surf. Sci. **178**, 578 (1986).
[21]J. A. Stroscio, S. R. Bare, and W. Ho, Surf. Sci. **148**, 499 (1984).
[22]J. A. Stroscio and W. Ho, Rev. Sci. Instrum. **57**, 1483 (1986).
[23]D. E. Peebles, H. C. Peebles, and J. M. White, Surf. Sci. **136**, 463 (1984).
[24]J. S. Villarrubia, Ph.D. thesis, Cornell University, 1987.
[25]J. A. Stroscio and W. Ho, Rev. Sci. Instrum. **55**, 1672 (1984).
[26]Y. Kim, H. C. Peebles, and J. M. White, Surf. Sci. **114**, 363 (1982).
[27]L. J. Richter, B. A. Gurney, and W. Ho, J. Chem. Phys. **86**, 477 (1987).
[28]F. Besenbacher, I. Stensgaard, and K. Mortenson, Surf. Sci. **191**, 288 (1987).
[29]L. J. Richter and W. Ho, J. Vac. Sci. Technol. A **5**, 453 (1987).
[30]L. J. Richter and W. Ho, Phys. Rev. B **36**, 9797 (1987).
[31]J. A. Stroscio, M. Persson, and W. Ho, Phys. Rev. B **33**, 6758 (1986).
[32]J. E. Reutt, Y. J. Chabal, and S. B. Christman, J. Vac. Sci. Technol. A **6**, 816 (1988).
[33]N. J. DiNardo and E. W. Plummer, J. Vac. Sci. Technol. **20**, 890 (1982).
[34]T. H. Upton and W. A. Goddard III, CRC Crit. Rev. Solid State Mater. Sci. **10**, 261 (1981).
[35]D. R. Hamann and P. J. Feibelman, Phys. Rev. B **37**, 3847 (1988).
[36]M. R. Barnes and R. F. Willis, Phys. Rev. Lett. **41**, 1729 (1978).
[37]A. M. Baró, H. Ibach, and H. D. Bruchmann, Surf. Sci. **88**, 384 (1979).
[38]M. A. Passler, B. W. Lee, and A. Ignatiev, Surf. Sci. **150**, 263 (1985).
[39]I. Stensgaard and F. Jakobsen, Phys. Rev. Lett. **54**, 711 (1985).
[40]C. Nyberg and C. G. Tengstål, Phys. Rev. Lett. **50**, 1680 (1983).
[41]P. R. Bevington, *Data Reduction and Error Analysis for the Physical Sciences* (McGraw-Hill, New York, 1969).
[42]E. G. McRae, Rev. Mod. Phys. **51**, 541 (1979).
[43]B. M. Hall, S. Y. Tong, and D. L. Mills, Phys. Rev. Lett. **50**, 1277 (1983).
[44]R. J. Behm, K. Christmann, and G. Ertl, Surf. Sci. **99**, 320 (1980).
[45]M. J. Puska and R. M. Nieminen, Surf. Sci. **157**, 413 (1985).
[46]S. Frøyen, S. Holloway, J. K. Nørskov, and B. Chakraborty, J. Electron. Spectrosc. Relat. Phenom. **38**, 313 (1986).
[47]I. Toyoshima and G. A. Somorjai, Catal. Rev.-Sci. Eng. **19**, 105 (1979); M. A. Morris, M. Bowker, and D. A. King, in *Comprehensive Chemical Kinetics,* edited by C. H. Bamford, C. F. H. Tipper, and R. G. Compton (Elsevier, Amsterdam, 1984), Vol. 19, pp. 1–179.
[48]S. W. Lovesey, *Condensed Matter Physics, Dynamic Correlations* (Benjamin/Cummings, Reading, 1980), pp. 126–135.
[49]P. Nordlander and S. Holmström, Surf. Sci. **159**, 443 (1985).
[50]B. E. Hayden, K. Prince, D. P. Woodruff, and A. M. Bradshaw, Phys. Rev. Lett. **51**, 475 (1983).
[51]J. P. Woods, A. D. Kulkarni, J. L. Erskine, and F. W. de Wette, Phys. Rev. B **36**, 5848 (1987).
[52]R. R. Cavanagh, R. D. Kelley, and J. J. Rush, J. Chem. Phys. **77**, 1540 (1982).
[53]J. J. Rush, R. R. Cavanagh, R. D. Kelley, and J. M. Rowe, J. Chem. Phys. **83**, 5339 (1985).
[54]J. C. Kimball, C. Y. Fong, and Y. R. Shen, Phys. Rev. B **23**, 4946 (1981).
[55]T. Holstein, R. Orbach, and S. Alexander, Phys. Rev. B **26**, 4721 (1982).
[56]J. C. Ariyasu and D. L. Mills, Phys. Rev. B **28**, 2389 (1983).
[57]Analytic forms for the bound-state wave function and energy is this model can be found in Ref. 54.
[58]M. Persson, Phys. Scr. **29**, 181 (1984).
[59]Second-order contributions to the scattering from the linear effective charge can also couple to the two-excitation sector. This second-order contribution has a negligible cross section for excitation of the two-phonon bound state and corresponds to the double loss (Ref. 56).
[60]J. Jortner and S. A. Rice, Phys. Rev. B **26**, 4727 (1982).
[61]F. Bogani, J. Phys. C **11**, 1283 (1978); **11**, 1297 (1978).
[62]S. Califano, *Vibrational States* (Wiley, London, 1976).
[63]R. A. DePaola, J. Hrbek, and F. M. Hoffmann, J. Chem. Phys. **82**, 2484 (1985).
[64]R. A. DePaola, J. Hrbek, and F. M. Hoffmann, J. Vac. Sci. Technol. A **2**, 1339 (1984).
[65]H. Pfnür, D. Menzel, F. M. Hoffmann, A. Ortega, and A. M. Bradshaw, Surf. Sci. **93**, 431 (1980).
[66]O. Madelung, *Introduction to Solid-State Theory* (Springer, Berlin, 1978).
[67]L. J. Richter, Ph.D. thesis, Cornell University, 1988.